AUTHOR'S RESPONSE TO EDITOR'S REVIEW

Manuscript: ACP-2018-981

Thank you again for commenting and spending time with this manuscript. We first reply on some major comments you both had and then, we reply to each of the comments separately. The comments by the editor and the referee are marked with bold font.

1 MAJOR CHANGES

To make to manuscript easier to read, we did rearranging and rewriting, we also removed part of the study according to your recommendations. All the changes are marked in red and you can find the marked up manuscript at the end of this document. The green color indicates that the place of the text had changed.

We made some changes to the sections: 1) We separated data processing from data analysis. 2) We combined the sections about seasonality of AOPs and the differences between the PM1 and PM10 and moved it as a subsection for the "Characterization of boreal aerosol particles". 3) We removed the size distribution analysis from the manuscript.

Now the sections are:

1 Introduction
2 Measurements and methods
- 2.1 The boreal research station SMEAR II
- 2.2 Instrumentation
  - 2.2.1. Measurements of AOPs
  - 2.2.2 Size distribution measurements
- 2.3 Data processing
  - 2.3.1 Corrections for the integrating nephelometer data
  - 2.3.2 Corrections for the Aethalometer data
- 2.4 Data analysis
  - 2.4.1 Intensive optical properties
  - 2.4.2 Aerosol radiative forcing efficiency
  - 2.4.3 Properties calculated from particle size distribution
  - 2.4.4 Data coverage and long-term trend analysis

3 Results and discussion
- 3.1 Characterization of boreal aerosol particles
  - 3.1.1 Seasonality of the AOPs
- 3.2 Long-term trends of the AOPs
- 3.3 Seasonality and long-term trend of the radiative forcing efficiency
- 3.4 Effect of excluding the moist data

4 Summary and conclusions

We emphasized in several parts of the manuscript that the data analysis was conducted for dry data and that the moist measurements were only taken into account in few special cases. We improved the discussion

about including the moist data in some special cases, which should make the difference between the dry and the moist data more clear.

2 RESPONSE TO EDITOR'S COMMENTS

2.1 EDITOR

GENERAL REMARKS

From the review by two referees and from my editor's review, the manuscript is still considered presenting high-relevance data and analyses of high interest for the research community. The authors have responded to the concerns raised by both referees, but still in an insufficient manner. I have sent the manuscript for a second review to one of the referees, who confirmed that many of the technical issues have been answered but the presentation quality is still considered poor.

Serious objections against publication arise still from the manner, the scientific results are presented. The core of the manuscript is the analysis of the long-term time series, which is of high relevance. However, there is no red line to follow in this manuscript. The presentation of results oscillates between different foci, which makes it hard to follow.

To help making the manuscript acceptable for publication, I suggest the following way forward:

(1) The time-series of PM10 data is well described but the reader has enormous difficulties identifying if the authors focus on dry or humid conditions. The confusion starts with the description of the sampling conditions in Section 2.2.1. Instead of combining all relevant information on sampling lines, aerosol drying etc. in this section the information is distributed among the Sections 2.2 and 2.3. This is in particular true for all topics related to relative humidity, humidity-driven particle growth and related impacts on aerosol optical properties.

We have now written all the parts that describe the sampling under section "2.2.1 Measurements of AOPs". We also improved the section 2.3.1, where we present the hygroscopic growth correction factor for scattering. We added there few sentences about the motivation why we use the f(RH) in the special cases.

Here, I suggest combining all information on particle sampling, including references to aerosol sampling at SMEAR, into Section 1. Already here it should be stated whether the manuscripts is focusing on dry or ambient aerosol conditions. Having said this, the specific treatment of samples at high RH conditions can be added. But it should be clear to the reader if the authors generally focus on dry or ambient conditions. The treatment of humid cases can then be introduced as special cases. Obviously, there have difficulties caused by the failed humidity control of the sampling during certain period, but the description of the difficulties and the resulting effects on the data analysis are presented at different positions of the manuscript. This needs to be presented in one section to allow the reader a clear assessment of the quality of data and deduced results.

Now all the information, which considers the sampling and instrumentation are in Sect. 2.2.1. We thought that maybe it is better that the introduction (Sect. 1) describes the motivation of the study rather than the sampling and the site. To underline that the data analysis was conducted for dry data, we added a sentence in Sect. 1, which states that we present the results for dry aerosol particles if not stated otherwise.

(2) To which conditions (dry, humid) do the reported optical properties refer to? For instance, in Section 2.3, the authors start directly with the introduction of the humidity growth factor, but it is not explained why. Here, a much clearer reasoning and description of the approach is needed. Having said this, it will be much clearer to follow the analyses. In particular, the discussion of the backscatter fraction needs to be removed at all since this factor was not corrected for humidity effects and thus treated completely different than the other optical properties. Thus, there is no way of comparing scattering and backscatter properties.

All the optical properties refer to dry conditions if not stated otherwise and we have now described this better in different sections. We moved the description of hygroscopic growth in to Sect. 2.2.1, which describes the sampling and explains why measurements of dry aerosol are preferred.

Instead of the parametrization presented by Zieger et al. (2015), we chose to use the parametrization by Andrews et al. (2006) presented in Sect. 2.3.1. Andrews et al. presented the parameters for backscattering as well. There was no drastic change in the results due to the different parameters used.

(3) The authors state correctly that trend analyses of time series of less than one decade duration have to be taken with care; see Section 3.2 on page 14. Why do the authors then present in detail the trend analysis of the PM1 time series? This is difficult to justify and contradicts with the statement made on trends from time series of less than 10 years duration. Here, I suggest removing the PM1 data from the trend analysis but present them as comparison to the PM10 trend results. This would give less weight to the PM1 results in terms of trends but still allows showing the difference to the PM10 results.

I still kept the results of PM1 trends in the text and in the Table 3 as a comparison, but I decreased their importance in the text. Their trends have the same sign as PM10 trends so they support the decreasing trend and show that the trends are not caused by changes in the measurement line (installation of the Nafion dryers in 2010).

(4) There are intensive properties discussed with respect to trends, but the trends are not significant. These facts need to be reflected in the description of the results; see Table 3 for quantities σ_{scat}, σ_{abs}, and refractive index real and imaginary parts. The interpretation of results needs to be softened since the trends are not sufficient.

We softened the interpretation of the trends that were not statistically significant.

(5) In the Figures there are clear statements missing to which fraction (PM10, PM1) the plots refer to. If the authors state at the very beginning on which fraction the manuscript is focusing at, these statements are no longer necessary.

We added statements of the particle fraction to figures, which were missing it.

(6) In Tables 1 and 2, the authors present statistical analyses of aerosol optical properties. Inspecting the tables in detail shows that there a large discrepancies between average values and median values. Such discrepancies are always a clear sign that Gaussian statistics is not applicable. I suggest reducing the statistical analysis to the robust analysis of median and percentiles. By doing this, any biases caused by extreme values are avoided and the results are much more stable.

We have corrected this in the text and in figures so that I always refer to the median values (only when comparing the RFE between different stations, we use the mean, because one of the studies did not report median values) . However, we prefer to keep the mean values in the table because it shows that the extensive AOPs do not follow the Gaussian statistics. We also added the following statement in the beginning of Sect. 3.1: *"Tables 1 and 2 show that for most of the variables the mean and the median values were quite different, which means that the data were not normally distributed. Therefore, we use the medians, which are not as sensitive to extreme values as the mean, to describe the characteristics of the AOPs."*

I am well aware that this further major revision may cause another large amount of work. On the other hand the paper has great potential and the trend analysis is of high interest for ACP but the presentation of the material requires a much clearer discussion of different topics and analysis results to improve overall readability and the delivery of a clear scientific goal/interest.

In summary, I encourage the authors to undertake this effort and accept the additional burden since the material is clearly worth it. I ensure further contribution and backing of the process to help publishing the manuscript. In case of questions or discussion the authors may contact me directly at a.petzold@fz-juelich.de.

Besides these general topics, I strongly encourage the consideration of the specific comments given by one referee in his 2nd review.

Thank you for the comments. We also took the comments given by the referee into account and the answers to those comments are presented below.

2.2 REFEREE

Comments of the referee are arranged by the old manuscript sections.

2.2.1 Introduction

The section is incomplete and not well structured.

The importance of AOPs for the estimation of the RF is not mentioned. Thus, the climatic motivations at the base of this study are unclear. The aerosol-cloud interaction is, presently, not of primary need. The description of the measurements and site (P2L16-30) is not of necessary, since it can be extensively described in the method section. Generally, I also find a serious lack of references. An introduction on aerosol trends, such as previous works, environmental policies, dimming, and brightening might underline the importance of your work.

We modified this section by doing some rearranging and by taking these comments into account. We added a mention of the RF and importance of knowing the AOPs in calculating this parameter. We modified the emphasis on the part considering the aerosol-cloud interaction, since it was not relevant. We moved the description of the sampling and part of the description of the station into Sect. 2. I still kept a part about SMEAR II, since it presents the motivation to study AOPs in a boreal forest. We also added references and text where we introduce long-term trends.

2.2.2 Measurements and methods

All measurements and data analysis are fully described. However, I would suggest to restructure and reorganize the different sections, starting from the titles. Try to be a more specific and attract the interest of the reader avoiding general titles such as "The field site", which could be changed into a more appealing "The SMEAR II boreal research station" (by the way here you have to insert the description given at P2L16-21).

We modified the titles and reorganized the sections (see Sect. 1 in this document). For example, we divided the data processing and analysis into separate sections.

EFR needs a separate section.

We fixed this.

Sections 2.3.4 and 2.5 can be merged.

We combined these two sections.

2.2.3 Overview of the data

Work on the titles and try to be a bit more original: "Characterisation of the boreal aerosol", or "Scandinavian background aerosol optical properties", etc... . It is important to define a target-topic for each section, I hardly see what you want to show here. The seasonal analysis can be used to describe the impact of different sources or the role of atmospheric processes on the AOPs.

We changed the title and also worked with the text. We combined here the seasonal variation of PM1/PM10.

2.2.4 Trends

A bit of rework on the red line and additional thinking on the climatic/environmental implications are needed.

We did also some rearranging and rewriting here to make the text more readable.

2.2.5 Aerosol optical properties and size distribution

As already indicated by me and the second reviewer, I do not understand the goal of this section. I would definitely give more priority to the interpretation of trends rather than to the size distribution. Moreover, too many variables are discussed making the section quite chaotic. Potentially, a reduced/simplified discussion on the aerosol size distribution can be introduced in 3.1 as part of the aerosol characterization.

We now removed this section. However, we added a figure about the seasonality of the size distribution, which shows that the b and α_{sca} depend on the accumulation mode.

2.2.6 Seasonal variation

As said before, I would move and merge it with 3.1

We created a subsection for the 3.1.

2.2.7 Variation between the PM10 and PM1 measurements

As already argued in the first review, this section is of scarce interest. In fact, a good part of the section is used to justify the differences from previous works (P20L27-P21L7) and the high uncertainty (P21L21-27).

We integrated this section into Sect. 3.1.1.

2.2.8 Radiative forcing efficiency

The section reads nice and might represent the final outcome of the manuscript. However, I have some suggestions:

a) The title can be improved: "Seasonality and trend of ".

We fixed this.

b) The text is very intricated, limiting the understanding.

We have now improved the text and made the differences between the $RFE_{H\&S}$, RFE_S, and $RFES_{,moist}$ more clear and easier to understand.

c) Figure 7 tells that humidity is very important in summer (hence hygroscopicity is a critical property of the aerosol in order to asses RF) and that optical properties have a smaller impact of RF compared to environmental factors. Considering these two messages and the high number of assumptions for the RFE calculation, Fig. 8 is quite approximative. A full investigation of the impact of AOPs on RF would need a full separated paper. Thus, I would suggest excluding, this time, Fig. 8 and the subsequent (very short) discussion.

This is true and we removed this figure and discussion from the manuscript.

2.2.9 Summary and conclusions

As a consequence of all the above comments, the conclusion section needs rethinking and rewriting.

We rewrote parts of the conclusion.

Over a ten-year record of aerosol optical properties at SMEAR II

Krista Luoma[1], Aki Virkkula[1,2], Pasi Aalto[1], Tuukka Petäjä[1] and Markku Kulmala[1]

[1]Institute for Atmospheric and Earth System Research, University of Helsinki, Helsinki, 00014, Finland
[2]Finnish Meteorological Institute, Helsinki, 00560, Finland

Correspondence to: Krista Luoma (krista.q.luoma@helsinki.fi), Aki Virkkula (aki.virkkula@fmi.fi)

Abstract. ~~The a~~Aerosol optical properties (AOPs) describe the ability of aerosols to scatter and absorb radiation at different wavelengths. Since ~~the~~ aerosol particles interact with the sun's radiation ~~from the sun~~, they ~~also have an~~ impact ~~on~~ the climate. Our study focuses on the long-term trends and seasonal variations of different AOPs measured at a rural ~~background station~~boreal forest site in Northern Europe. To explain the observed variations in the AOPs, we also analyzed changes in the aerosol size distribution. AOPs of particles smaller than 10 µm (PM10) and 1 µm (PM1) have been measured at SMEAR II, in Southern Finland, since 2006 and 2010, respectively. For ~~the~~ PM10 particles, the median values of the scattering and absorption coefficients, single-scattering albedo, and backscatter fraction at λ = 550 nm were ~~15.2~~9.8 Mm^{-1}, ~~2.1~~1.3 Mm^{-1}, 0.~~87~~88 and 0.14. The median scattering and absorption Ångström exponents at the wavelength ranges 450–700 nm and 370–950 nm were 1.~~80~~88 and 0.~~95~~99, respectively. We found ~~S~~statistically significant trends ~~were found for example~~ for the PM10 scattering and absorption coefficients, single-scattering albedo, and backscatter fraction, and the slopes of these trends were -0.32 Mm^{-1}, -0.086 Mm^{-1}, 2.2·10^{-3}, and 1.3·10^{-3} per year. The tendency for the extensive AOPs to decrease correlated well with the decrease in aerosol number and volume concentration. The tendency for the ~~single-scattering albedo and~~ backscattering fraction and single-scattering albedo ~~-~~to increase indicates that the aerosol size distribution consist of less larger particles and that aerosols absorb relatively less light than before. The trends of the single-scattering albedo and backscattering fraction influenced the ~~effective~~ aerosol radiative forcing efficiency, indicating that the aerosol particles are scattering the radiation more effectively back into space.

1 Introduction

Aerosols affect the radiative balance of the atmosphere both directly by aerosol–radiation interactions (ARI), i.e., by scattering and absorbing solar radiation and by absorbing and emitting terrestrial infrared radiation, and indirectly by aerosol–cloud interactions (ACI), i.e., by influencing the properties and processes of clouds (Charlson et al., 1992; Lohmann and Feichter, 2005; Ramanathan et al., 2001; Stocker, 2013)~~(Charlson et al., 1992; Lohmann and Feichter, 2005; Ramanathan et al., 2001).Aerosol particles directly affect the climate by scattering and absorbing the shortwave radiation from the sun (ARI, *aerosol–radiation interaction*).~~ The uncertainty of the estimated radiative forcing of climate by ACI is larger than that by ARI but also the latter is substantial (Stocker, 2013)~~{Stocker, 2013 #153}{Stocker, 2013 #153@@author-year}~~. Both ARI and ACI have been shown to be responsible of dimming, the reduction of solar radiation received at the surface of the Earth (Wild,

2009, 2012; Stocker et al., 2013). Dimming and brightening have been shown to be often reconcilable with the trends in anthropogenic emissions of aerosols and their precursors and atmospheric aerosol loadings (Wild, 2012).

Aerosol optical properties (AOPs) describe the ability of aerosol particles to absorb and scatter radiation at different wavelengths. Knowing how aerosol particles interact with radiation is essential in determining the direct effect that aerosols have on the climate. ~~Aerosol particles can either have a warming or cooling effect on the climate, depending on the optical properties of the aerosol particles and the surface below the aerosol layer.~~The direct effect of aerosol can either be warming or cooling, depending on the AOPs and the properties of the surface below the aerosol layer (Haywood and Shine, 1995). ~~Aerosol particles also affect the climate via aerosol–cloud interactions (ACIs) since aerosol particles may act as cloud condensation nuclei (CCN). By functioning as CCN, aerosol particles also affect the optical properties of the cloud . The more CCN are available, the smaller and more numerous are the cloud droplets. Clouds with more droplets scatter light more efficiently, so they have a larger cooling effect than clouds that have fewer droplets . Clouds with smaller droplets have longer lifetimes, since it requires more time for the cloud droplets to grow to the size of rain drops . Longer lifetimes also increase the cooling effect of the clouds.~~ Determining the global radiative forcing (RF) related to the direct effect of aerosol particles has vast uncertainties (Stocker, 2013)~~{Stocker, 2013 #153}~~, which are due to the wide spatial and temporal variations of the number concentration, chemical composition and size distribution of aerosol particles, so it is challenging to consider them in climate models.

~~The aerosol optical properties (AOPs) describe how much the particles scatter and absorb radiation at different wavelengths. It is essential to know how the aerosol particles interact with radiation to determine the direct effect on the climate. The extensive optical properties, such as scattering and absorption coefficients, are dependent on the mass and/or volume of the particles and also on their size distribution and chemical composition. Intensive properties, however, are not dependent on the amount of aerosol but on the properties of the particles, such as the size distribution and composition. Intensive properties are calculated from the scattering, backscattering and absorption measurements at different wavelengths. Therefore, by measuring the AOPs at different wavelengths, we can also obtain indirect information on the size distribution and chemical composition of the aerosol particles.~~

Making long-term observations of aerosol concentrations and properties at several regionally representative sites is necessary to understand and quantify the global influence of aerosols (e.g. Laj et al., 2009; WMO/GAW, 2012; Weatherhead et al., 2018; Andrews et al., 2019). There are several networks of stations where such measurements are conducted, both global and regional (Pandolfi et al., 2018; WMO/GAW, 2012). The goal of the Global Atmosphere Watch (GAW) is to ensure long-term measurements of atmospheric variables in order to detect trends and reasons for those trends (WMO/GAW, 2012). This can be considered as the goal of all long-term aerosol measurements. Trends in AOPs can also be used as indicators of emission control measures (Pandolfi et al., 2018). Recently Collaud Coen et al. (2013) presented trends of in-situ AOPs at 24 GAW and

IMPROVE stations, Sherman et al. (2015) presented trends of AOPs at four North American surface monitoring sites, Lihavainen et al. (2015) presented trends of AOPs at the Pallas GAW station, and Pandolfi et al. (2018) presented trends of scattering coefficients at 28 ACTRIS observatories located mainly in Europe.

Here we present the results of long-term measurements of AOPs at SMEAR II (Station for Measuring Ecosystem–Atmosphere Relations; Hari and Kulmala, 2005). The location represents the typical conditions of a boreal forests (Hari et al., 2013), which are a source of new aerosol particles formed in gas-to-particle conversions (Kulmala et al., 2004; Kulmala et al., 2013). Boreal forests (also known as Taiga) cover approximately 30 % of the world's forests and 8 % of the Earth's surface, so they greatly affect the global radiation budget.

AOPs at SMEAR II have previously been discussed by Virkkula et al. (2011), Zieger et al. (2015), and Pandolfi et al. (2018). Virkkula et al. (2011) presented the scattering and absorption data from a 3-year period (2006–2009), Zieger et al. (2015) presented the hygroscopic properties of AOPs measured during a campaign in May – Augusts in 2013, and Pandolfi et al. (2018) included SMEAR II in the paper on aerosol scattering at 28 ACTRIS stations. At SMEAR II, the study by Pandolfi et al. (2018) involved nephelometer data, from 2006 to 2015, but did not include absorption data.

Long time series (2006–2017) of both scattering and absorption together at SMEAR II have not been presented before. The aim of this study is to present the characteristics and the temporal variation, especially trends, of AOPs at SMEAR II in this period. We also present the optical properties of particles smaller than 1 µm in diameter (PM1) that were presented neither by Virkkula et al. (2011) nor Pandolfi et al. (2018). To be consistent with the GAW recommendations (WMO/GAW, 2016), we present the results for dry aerosol particles (RH < 40 %), if not stated otherwise.

~~In situ measurements of AOPs have been conducted at SMEAR II (Station for Measuring Ecosystem–Atmosphere Relations; Hari and Kulmala, 2005) in Hyytiälä, Finland since 2006. SMEAR II is located in the middle of a pine forest and represents the atmospheric conditions typically found in boreal forests . Boreal forests are sources for new aerosol particles that are formed in a gas-to-particle conversions . Boreal forests (also known as Taiga) cover approximately 30 % of the world's forests and 8 % of the earth's surface, so they greatly affect the global radiation budget.~~

~~The measurements of AOPs were started for aerosol particles smaller than 10 µm in diameter (PM10). The PM10 measurements are sensitive to coarse particles that are typically primary and originated from natural sources, such as soil dust and sea salt. To obtain additional information about submicron particles, parallel measurements of AOPs for PM1 were launched in June 2010. Motivation to measure also PM1 particles is that secondary aerosols (both natural and anthropogenic), and anthropogenic primary aerosols are typically submicron particles. Having measurements for different cut-offs makes the measurements also more comparable between different stations, since stations might use different cut-off sizes. To study the~~

~~causalities between the AOPs and the size distribution, we have also included the measurements of aerosol size distribution to our study.~~

~~Here, we present the observed temporal variation and trends of the AOPs at SMEAR II. These AOPs have been previously discussed by and . used the integrating nephelometer and the aethalometer data from a 3-year period (2006–2009). compared the aerosol scattering measurements that were conducted at different measurement sites in Europe. At SMEAR II, the study involved nephelometer data, from 2006 to 2015. However, these articles determined the AOPs of the PM10 particles only, and did not include absorption data. Long time series (2006–2017) of the measurements of both scattering and absorption together at SMEAR II have not been presented before, nor have the optical properties of the PM1 particles.~~

2 Measurements and methods

2.1 The boreal research station ~~field site~~SMEAR II

The measurements were conducted at SMEAR II (Station for Measuring Ecosystem–Atmosphere Relations; Hari and Kulmala, 2005). SMEAR II is located in Hyytiälä, Southern Finland (61° 51' N, 24° 17' E, 181 m above sea level.), in ~~the~~ middle of a forest that consists mostly of Scots pine (*Pinus sylvestris* L.) trees (Hari et al., 2013). SMEAR II is classified as a rural measurement station and there are no large pollution sources nearby the station. ~~The measurements presented here were conducted at the SMEAR II station in Hyytiälä, southern Finland (61° 51' N, 24° 17' E, 181 m above sea level.). SMEAR II is located in the middle of a forest that consists mostly of Scots pine (*Pinus sylvestris* L.) trees (Hari et al., 2013).~~ ~~T~~The nearest larger cities, ~~,~~ Tampere (220 000 inhabitants) and Jyväskylä (140 000 inhabitants), are located about 60 ~~km~~ and 100 km from the measurement station. Otherwise, the area is sparsely populated ~~and there are no large pollution sources nearby the station~~.

2.2 Instrumentation

2.2.1 Measurements of ~~aerosol optical properties~~AOPs

The data were measured between 21 June 2006 and 31 December 2017. Measurements of AOPs ~~have been measured~~ at SMEAR II ~~since~~started in ~~June~~ 2006. for aerosol particles smaller than 10 µm in diameter (PM10). The PM10 measurements are sensitive to coarse particles that are typically primary and originated from natural sources, such as soil dust and sea salt. To obtain additional information about submicron particles, parallel measurements of AOPs for PM1 were launched in June 2010. Motivation to measure also PM1 particles is that secondary aerosols (both natural and anthropogenic), and anthropogenic primary aerosols are typically submicron particles. Having measurements for different cut-offs makes the measurements also more comparable between different stations, since stations might use different cut-off sizes. This is also in line with the GAW

recommendation that the aerosol supplied to the nephelometer should be size-segregated to determine the total (< 10 µm diameter) and submicron aerosol light scattering coefficient (WMO/GAW, 2003).

AOPs are often divided into two different categories: extensive and intensive. Extensive AOPs, such as scattering and absorption coefficients and aerosol optical depth depend on the amount of the particles whereas the intensive AOPs depend on the nature of the aerosol, such as size, shape and chemical composition. Intensive AOPs describe for instance the fraction of aerosol light extinction due to scattering (single-scattering albedo), the wavelength dependence of scattering and absorption (Ångström exponents), and the angular dependence of scattering (hemispheric backscatter fraction) (Ogren, 1995; Sheridan and Ogren, 1999). Intensive properties are calculated from the scattering, backscattering and absorption measurements at different wavelengths. The Ångström exponent of scattering and backscatter fraction depend on particle size so by measuring the AOPs at different wavelengths, we can also obtain indirect information on the size distribution.

~~AOPs have been measured at SMEAR II since June 2006.~~ The ~~measurements of aerosol scattering~~extensive AOPs, which are scattering, backscattering and absorption coefficients (σ_{sca}, σ_{bsca} and σ_{abs}), were ~~conducted~~ measured at several wavelengths using an integrating nephelometer (TSI model 3563) and an aethalometer (Magee Scientific model AE-31), since 2013 also with a Multi-Angle Absorption Photometer (MAAP, Thermo Scientific model 5012). The integrating nephelometer measures scattering and backscattering at blue, green and red wavelengths (450, 550 and 700 nm) and the aethalometer measures absorption at seven wavelengths ranging from the ultraviolet to the near-infrared (370, 470, 520, 590, 660, 880 and 950 nm). Here, absorption data from the AE-31 and scattering data from the TSI3563 were used since they have the longest time series, and an important part of our discussion is the analysis of trends. We used the MAAP data in determining a multiple scattering correction factor for the Aethalometer to get more accurate absorption measurements (see Sect. 2.3.2).

~~Both s~~Scattering and absorption measurements were recorded at~~with~~ a 5-minute resolution before June 2010 and after that with a 10-minute resolution. From June 2006 to June 2010, the measurements were conducted for the PM10 particles only and since June 2010 also for the PM1 particles. The sample air wa~~s~~s taken through a PM10 inlet (Digitel, Low volume PM10 inlet) and led alternatingly either directly to the instruments or via an impactor that removes particles larger than 1 µm in diameter. The path of the sample alternated every ten minutes.

The aerosol hygroscopic growth is often significant when relative humidity (RH) increases above ~40 ± 5% and therefore the World Meteorological Organization and Global Atmosphere Watch (WMO and GAW) recommends aerosol monitoring stations to keep sample air RH lower than that (WMO/GAW, 2016). Until March 2010, the integrating nephelometer and the aethalometer measured sample air that was not dried with any external driers. The sample air was only dried passively by letting it warm from the outdoor temperature to the room temperature (about 22 °C). During winter, RH remained below 40 %, since the difference between the outdoor and the room temperatrue was high. In summer, however, the temperature

difference was a lot lower. Therefore, sometimes in summer, RH of the sample exceeded the 40 % limit. If the RH was above 40 %, the data were flagged as invalid and omitted from the data analysis, if not stated otherwise. When we discuss about dry aerosols, we mean that the measurements were condcucted for sample air that had RH < 40 %.

2.2.2 ~~Size distribution measurements~~Measurements of aerosol size distribution

To study the causalities between the AOPs and the aerosol size distribution, we included the measurements of aerosol size distribution in our study. ~~In addition to the AOPs, particle size distribution data were used in the analyses below.~~ The size distributions were measured with a Twin Differential Mobility Particle Sizer (TDMPS) in the size range 3–1000 nm (Aalto et al., 2001) and a TSI Aerodynamic Particle Sizer (APS, Model 3321) in the size range 0.53–10 µm. In the overlapping range of the TDMPS and the APS, we used the number concentrations from the TDMPS ~~were used~~ up to 700 nm. The TDMPS and~~,~~ APS located in the same building as the~~,~~ integrating nephelometer and the aethalometer ~~are located in the same measurement building~~. The TDMPS and APS ha~~ve~~d their own individual measurement lines. In the TDMPS measurement line, there was~~is~~ an inlet removing~~that removes~~ particles larger than 1 µm. There wa~~i~~s no active drying system in the TDMPS sample line to prevent particle losses. However, the sheath flows, ~~which are u~~used in the TDMPS system, wea~~r~~e dried (RH < 40 %) so the particles ~~are~~ were sampled in dry conditions. In the APS measurement line there ~~is~~ was a pre-impactor that remove~~s~~d~~s~~ particles larger than 10 µm. The APS ~~has~~ had its own dryer that heated~~s up~~ the sample air to 40 °C. This temperature might have evaporate some semivolatile compounds, for instance ammonium nitrate but this is mainly an issue of urban sites (e.g. Bergin et al. 1997), whereas at the forest site in Hyytiälä low-volatile organic compounds are common (Ehn et al., 2014). Nevertheless, semivolatile aerosol particles are typically secondary particles smaller than 1 µm in diameter so evaporation of them does not have a large effect on the APS measurements.

2.3 Data processing

~~The data used in this study were measured between 21 June 2006 and 31 December 2017.~~ All the optical data were quality assured manually and averaged for one~~1~~ hour~~ periods~~. ~~Note that Virkkula et al. (2011) followed the earlier RH recommendation: they calculated AOPs using data measured at RH < 50%. In addition, they also presented results from data measured at all RH. This affects comparisons of the results presented in this work.~~

All the optical data were ~~also~~ converted from ambient conditions to the standard temperature and pressure (STP) conditions (1013 hPa, 0 °C). We excluded the data from further analysis if the internal RH in any of the optical instruments exceeded 40 %, if not stated otherwise.

2.3.1 ~~Scattering data~~Corrections for the integrating nephelometer data

Both σ_{sca} and σ_{bsca} ~~total scattering and backscattering coefficients~~ measured with the nephelometer were corrected for the truncation error according to Anderson and Ogren (1998). The truncation correction uses the Ångström exponent (see Sect. 2.~~4~~1~~3~~.~~1~~3~~) calculated from the uncorrected data.

Sherman et al. (2015) presented a well documented analysis for determining the uncertainty of the different AOPs. They determined a total fractional uncertainty of 9.2 % and 8.9 % (8.0 % and 8.1 %) for PM10 (PM1) σ_{sca} and σ_{bsca}.

~~To test, if excluding the moist data had a large effect on the AOPs and their trends, we included the periods of high humidity (RH > 40 %) in some of the analyses. However, in these cases we corrected the scattering data, which was flagged due to too high RH, to dry conditions by using the scattering enhancement factor *f*(RH). *f*(RH) describes the increase of σ_{sca} with increasing RH~~

~~$$f(\mathrm{RH}) = \frac{\sigma_{sca}(\mathrm{RH})}{\sigma_{sca}(\mathrm{RH=\ dry})}, \quad (1)$$~~

~~*f*(RH) is the ratio of σ_{sca} measured at high RH and at dry conditions. The *f*(RH) can be described by empirical relationship~~

~~$$f(\mathrm{RH}) = q\left(1 - \frac{\mathrm{RH}}{100\ \%}\right)^{-\gamma}, \quad (2)$$~~

~~with a parametrization presented by for aerosol particles measured at SMEAR II in summer. They determined mean values for q and γ that were 0.96 ± 0.07 and 0.24 ± 0.07 at red wavelength (450 nm), 1.01 ± 0.05 and 0.25 ± 0.07 at green wavelength (525 nm), and 1.01 ± 0.05 and 0.30 ± 0.08 at red wavelength (635 nm). We used this parametrization, when the RH was higher than 40 %. presented parameterization for total scattering only so we did not correct the σ_{bsca} to dry condition.~~

~~This parametrization was also used for calculating the radiative forcing efficiency (see Sect. 2.3.3) in ambient RH.~~

Generally, in this study, the results are presented for dry aerosol (RH < 40 %), and therefore the hygroscopic growth had no notable effect on scattering. However, we had to take the effect of hygroscopic growth on scattering into account in two special cases: 1) to test if excluding the moist data (RH > 40 %) had a notable effect on the average AOPs and their trends; and 2) to calculate the aerosol radiative forcing efficiency (see Sect. 2.4.2) for ambient RH conditions.

In these special cases, we used a scattering enhancement factor *f*(RH) to estimate the effect of RH on scattering. *f*(RH) describes the increase of σ_{sca} with increasing RH

$$f(\mathrm{RH}) = \frac{\sigma_{sca}(\mathrm{RH})}{\sigma_{sca}(\mathrm{RH=\ dry})}. \quad (1)$$

f(RH) is the ratio of σ_{sca} measured at high RH and at dry conditions. The *f*(RH) can be described by empirical relationship

$$f(\mathrm{RH}) = q\left(1 - \frac{\mathrm{RH}}{100\ \%}\right)^{-\gamma}, \quad (2)$$

with a parametrization presented by Andrews et al. (2006). They determined mean values for q and γ that were 0.84 ± 0.10 and 0.37 ± 0.15 for σ_{sca} and 0.96 ± 0.16 and 0.12 ± 0.15 for σ_{bsca}. Andrews et al. (2006) presented the parameterization at 550 nm so we corrected only the σ_{sca} and σ_{bsca} at green wavelength. Andrews et al. (2006) used a four-year-long dataset measured at the Southern Great Plains near Lamont, in Oklahoma, US. We decided to use this parametrization, since they provided the parametrization for both σ_{sca} and σ_{bsca}. Also, the measurements were conducted for continental aerosol, which is closer to aerosols in a boreal forest than the mixtures of pollution, dust, sea salt, and volcanic aerosol, for which Carrico et al. (2003) presented the parametrization for both σ_{sca} and σ_{bsca}. Zieger et al. (2015) determined scattering enhancement at SMEAR II in summer and obtained somewhat different values: q = 1.01 ± 0.05 and γ = 0.25 ± 0.07. This would have suited our needs very well, but the q and γ were determined only for σ_{sca} and not for σ_{bsca}, which is why we did not use this parametrization here.

In testing whether excluding the moist data has an effect on the AOPs, we performed the analysis also to a data set, where we included the periods of high humidity (RH > 40 %), but estimated the moist data (RH > 40 %) to dry conditions by using the *f*(RH). We used the *f*(RH) also in calculating the aerosol radiative forcing efficiency in ambient conditions, for which the dry σ_{sca} and σ_{bsca} were converted to ambient RH.

2.3.2 ~~Absorption~~ Corrections for the Aethalometer~~data~~ data

The reported flow by the aethalometer was corrected by comparing the flow with the weekly flow measurements conducted at the station. The correction was applied by using a moving average of these measurements (see Sect. S3~~2~~.1). An average spot size diameter of 8.3 ± 0.2 mm was measured from the old aethalometer filters by using a loupe measuring scale magnifier (Eschenbach) with 0.1 mm accuracy and it was used instead of the spot size reported by the aethalometer.

~~Here, w~~We corrected the Aethalometer data by using the correction algorithm described by Collaud Coen et al. (2010)

$$\sigma_{\mathrm{abs},i} = \frac{\sigma_{\mathrm{ATN},i} - a_{s,i}\bar{\sigma}_{\mathrm{sca},s,i}}{C_{\mathrm{ref}}\, L_{s,i}}, \quad (3)$$

where

$$L_{s,i} = \left(\frac{1}{l\left(1-\bar{\omega}_{0,s,i}\right)+1} - 1\right) \cdot \frac{\mathrm{ATN}_i}{50\ \%} + 1, \quad (4)$$

and

$$a_{s,i} = \bar{\zeta}_{\mathrm{sca},s,i}^{d-1} \cdot c \cdot \lambda^{-\bar{\alpha}_{sca,s,i}\cdot(d-1)}. \quad (5)$$

In Eqs. 3 – and 45, the subscript *i* indicates the number of the measurement and the subscript *s* indicates the average properties of the aerosol particles that are embedded in the filter spot. The parameters with an overover lined parametersbar are the mean values from the start of the filter spot to the *i*th measurement. In Eq. 3, the σ_{ATN} is the attenuation coefficient reported by the Aethalometer, *a* is the scattering correction parameter, C_{ref} is the multiple scattering correction factor, and *L* is the loading correction function. In Eq. 4, the ω_o is the single scattering albedo (see Sect. 2.43.13) and the ATN is the light attenuation through the filter spot in percentages. In Eq. 5 the ζ_{sca} is the proportionality constant of the wavelength power law dependence of σ_{sca} and α_{sca} is the Ångström exponent of the σ_{sca} (see Sect. 2.43.13). For *l*, *d*, and *c* we used values 0.74, 0.564 and $0.329 \cdot 10^{-3}$ respectively. For scattering correction, we used measured σ_{sca} values that were interpolated and extrapolated to the AE-31 wavelengths. Note that most of the symbols used for the variables are different from Collaud Coen et al. (2010). The reason is that in the present work the symbols are used for other variables below.

The C_{ref} was determined by comparing the Aethalometer data, that was corrected only for the filter loading artefact, against the reference absorption coefficient ($\sigma_{abs,ref}$) measured by the MAAP.

$$C_{\mathrm{ref}} = \frac{\sigma_{\mathrm{ATN}}}{L \cdot \sigma_{\mathrm{abs,ref}}}. \quad (6)$$

The resulted median value for C_{ref} was 3.19, with a standard deviation of 0.67.

The uncertainty of the σ_{ATN} was determined according to Backman et al. (2017)

$$\frac{\delta\sigma_{\mathrm{ATN}}}{\sigma_{\mathrm{ATN}}} = \sqrt{f_{\mathrm{A}}^2 + f_{\mathrm{Q}}^2 + \left(\frac{\delta\sigma_{\mathrm{ATN,zero}}\Delta t_{\mathrm{zero}}}{\sigma_{\mathrm{ATN}}\Delta t_{\mathrm{avg}}}\right)^2}, \quad (7)$$

where the f_A and f_Q are the fractional uncertainties of the Aethalometer spot size and flow, which we determined to be 4.9 % and 1.5 % respectively; $\delta\sigma_{ATN,zero}$ is the standard deviation of the zero measurements; Δt_{zero} is the averaging time of the zero measurements; and Δt_{avg} is the averaging time of the measuremetnsmeasurements. For the uncertainty of σ_{abs} we took into account the fractional uncertainty of the C_{ref}, thatwhich was f_C = 21 %

$$\frac{\delta\sigma_{\mathrm{abs}}}{\sigma_{\mathrm{abs}}} = \sqrt{\left(\frac{\delta\sigma_{\mathrm{ATN}}}{\sigma_{\mathrm{ATN}}}\right)^2 + f_C^2}. \quad (8)$$

At 520 nm, the uncertainty of σ_{abs} ranges from 22 % to 24 % if the σ_{ATN} varies from 14.2 Mm^{-1} to 1.3 Mm^{-1}, which are the 10th and 90th percentiles of σ_{ATN}. In this estimation of uncertainty, we did not take the uncertainty of scattering correction into account.

In calculating the single-scattering albedo (see Sect. 2.4.1) and in iterating the complex refractive index (see Sect. 2.4.3), the absorption data had to be interpolated to the same wavelength with the scattering measurements. The absorption data were

then interpolated to the blue, green, and red wavelengths (450, 550, and 700 nm), using the Ångström exponent (α) described in Eqs. 11 and 12.

~~Note that Virkkula et al. (2011) followed the earlier RH recommendation: they calculated AOPs using data measured at RH < 50%. In addition, they also presented results from data measured at all RH. This affects comparisons of the results presented in this work.~~

~~To test, if excluding the moist data had a large effect on the AOPs and their trends, we included the periods of high humidity (RH > 40 %) in some of the analyses. However, in these cases we corrected the scattering data, which was flagged due to too high RH, to dry conditions by using the scattering enhancement factor *f*(RH). *f*(RH) describes the increase of σ_{sca} with increasing RH~~

~~$$f(\mathrm{RH}) = \frac{\sigma_{sca}(\mathrm{RH})}{\sigma_{sca}(\mathrm{RH=\ dry})}, \quad (1)$$~~

~~*f*(RH) is the ratio of σ_{sca} measured at high RH and at dry conditions. The *f*(RH) can be described by empirical relationship~~

~~$$f(\mathrm{RH}) = q\left(1 - \frac{\mathrm{RH}}{100\ \%}\right)^{-\gamma}, \quad (2)$$~~

~~with a parametrization presented by for aerosol particles measured at SMEAR II in summer. They determined mean values for q and γ that were 0.96 ± 0.07 and 0.24 ± 0.07 at red wavelength (450 nm), 1.01 ± 0.05 and 0.25 ± 0.07 at green wavelength (525 nm), and 1.01 ± 0.05 and 0.30 ± 0.08 at red wavelength (635 nm). We used this parametrization, when the RH was higher than 40 %. presented parameterization for total scattering only so we did not correct the σ_{bsca} to dry condition.~~

~~This parametrization was also used for calculating the radiative forcing efficiency (see Sect. 2.3.3) in ambient RH.~~

2.4 Data analysis

Here we describe the intensive optical properties, the aerosol radiative forcing efficiency, and parameters derived from the size distribution measurements.

2.~~3.3~~ 4.1 Intensive optical properties

The extensive AOPs, ~~extensive AOPs, which are the scattering, backscattering, and absorption coefficients (~~σ_{sca}, σ_{bsa}, and σ_{abs}~~),~~ , were used to calculate intensive properties presented in detail below.

The single-scattering albedo (ω_0) describes how much of the total light extinction (sum of σ_{sca} and σ_{abs}) caused by the aerosol particles is due to scattering:

$$\omega_0 = \frac{\sigma_{sca}}{\sigma_{sca} + \sigma_{abs}}. \quad (9)$$

The ω_0 can be linked with the source and chemical composition of the aerosol particles. High values of ω_0 mean that the aerosol particles are mostly scattering and are light in color. Darker aerosol particles, which have a lower ω_0, have a relatively higher mass fraction of absorbing material, such as soot, which ~~that~~ is emitted in combustion processes.

The backscatter fraction (b) describes how much aerosol particles scatter radiation in the backward hemisphere compared with the total scattering

$$b = \frac{\sigma_{bsca}}{\sigma_{sca}}. \quad (10)$$

The angular dependency of particle scattering ~~is dependent~~depends mostly on the particle size. The ~~value of~~ b is smaller for a size distribution that consists of larger particles, since large particles scatter light heavily in the forward direction and thus b can be used as an indicator of the shape of the particle size distribution. The b is an ~~especially~~ important ~~property~~ variable for modeling the direct effect of aerosol particles on the climate, since it is used to describe how much sunlight is scattered upwards back into space.

The Ångström exponent (α) is used to describe the wavelength (λ) dependency of a certain optical property (σ) (Ångström, 1929)

$$\alpha = -\frac{\ln\frac{\sigma_1}{\sigma_2}}{\ln\frac{\lambda_1}{\lambda_2}}. \quad (11)$$

After calculating α, the optical property can be extrapolated or interpolated into different wavelengths

$$\sigma_1 = \sigma_2 \left(\frac{\lambda_1}{\lambda_2}\right)^{-\alpha}. \quad (12)$$

In this study, α values were calculated for σ_{sca} and σ_{abs} to obtain α_{sca} and α_{abs}~~.~~.

Scattering~~Since light scattering~~ by aerosol particles ~~is highly d~~dependen~~d~~t on the relation between the sizes of the particles and the wavelength of the radiation, ~~particle size,~~ therefore also α_{sca} is ~~also~~ used as an indicator of the particle size distribution. The α_{sca} ~~and~~ is larger for the smaller particles, since they have a stronger wavelength dependency. If α_{sca} is larger than 2, the volume distribution is typically dominated by particles smaller than 0.5 µm, and if α_{sca} is smaller than 1, larger particles (physical diameter D_p > 0.5 µm) predominate in the distribution (Schuster et al., 2006). In comparison to b, α_{sca} is more sensitive to the coarse mode particles (e.g. Collaud Coen et al., 2007). However, for multimodal size distributions this relationship is not quite unambiguous, as discussed by, for example, Schuster et al. (2006) and Virkkula et al. (2011).

The ~~value of~~ α_{abs} depends also on the chemical composition, coating, and size of the particles, even though the chemical composition is generally considered ~~to be the~~as a more important factor. The α_{abs} is usually used to identify black carbon (BC) and brown carbon (BrC) particles. The BC particles are ~~highly absorbing~~absorb radiation effectively ~~aerosol particles~~at all wavelengths; ~~and~~ the BrC particles, which ~~are considered to~~ consist of ~~some~~ organic carbon compounds, ~~that~~ absorb light ~~more~~ strongly at short~~er than long~~ wavelengths, but not at longer wavelengths. If the particles consist purely of BC, the absorption would have a wavelength dependence~~y~~ of approximately λ^{-1} and α_{abs} would be equal to unity. However, if the particles also consist of material that absorbs light only at ultraviolet wavelengths, α_{abs} would be larger than ~~1~~one. In ageing processes, the BC particles may become coated by some purely scattering material, such as sulfuric acid or ammonium sulfate, or by slightly absorbing organic material (Schnaiter et al., 2005; Zhang et al., 2008). The coating greatly affects the absorption wavelength dependency, and thus the division into BC and BrC by considering only the α_{abs} is not that simple. If the sizes of the BC particles and the thickness and complex refractive index (m) of the coating are not known, it is challenging to use α_{abs} to describe the chemical composition of the particles (Gyawali et al., 2009; Lack and Cappa, 2010). In spite the fact that the α_{abs} depends also on the coating, the absorption wavelength dependency is often used to describe the source of the BC (Sandradewi et al., 2008; Zotter et al., 2017). The source apportionment assumes that there are BC emissions only from traffic and wood burning and that the BC from these sources has a specific wavelength dependency.

The estimated uncertainties for the intensive AOPs are presented in Sect. S4~~3~~ in the supplementary material. The uncertainties were calculated according to Sherman et al. (2015).

2.4.2 Aerosol radiative forcing efficiency

To investigate how the AOPs at SMEAR II would affect the climate, the aerosol radiative forcing efficiency ($\Delta F\delta^{-1}$ or RFE) was ~~also~~ calculated. The RFE is a simplified formula that describes how large a difference the aerosol particles would make to the radiative forcing (ΔF or RF) per unit of aerosol optical depth (δ) (Sheridan and Ogren, 1999)

$$\frac{\Delta F}{\delta} = -DS_0T_{at}^2\omega_0\beta(1-A_c)\left[(1-R_s)^2-\left(\frac{2R_s}{\beta}\right)\left(\frac{1}{\omega_0}-1\right)\right]. \quad (13)$$

RFE does not take into account that the properties and amount of aerosol particles vary vertically in the atmospheric column. In the Eq. 13, D is the fractional day length, S_0 the solar constant, T_{at} the atmospheric transmission, A_C the fractional cloud amount, and R_S the surface reflectance for which the following constants were used respectively: D = 0.5, S_0 = 1370 Wm^{-2}, T_{at} = 0.76, A_C = 0.6 and R_S = 0.15. The values were according to Haywood and Shine (1995), who used these values independent of wavelength in calculating the ~~AF~~RF. Sheridan and Ogren (1999) used these same constants later in calculating the RFE at 550 nm and~~.~~ ~~I~~in this study we determine the RFE also at 550 nm. The factor β is the upscatter fraction and is calculated by using the b (Delene and Ogren, 2002)

$$\beta = 0.0817 + 1.8495b - 2.9682b^2. \quad (14)$$

It must be noted that Eq. 14 does not take into account the variation in the sun's zenith angle.

As stated by Sherman et al. (2015), the purpose of determining the RFE is to provide ~~a~~ means for comparing the intrinsic aerosol forcing efficiency of aerosols measured at different sites. We calculated the RFE by using the same constant values to have results comparable with other studies in very different types of environments (e.g. Sheridan and Ogren, 1999; Andrews et al., 2011; Sherman et al., 2015; Shen et al., 2018) and to study how the RFE changes with varying ω_0 and b. W~~Here w~~e refer the RFE that was calculated by using the above-mentioned constant values as $RFE_{H\&S}$. It must be noted that ω_0 and b used in Eq. 13 are defined for dried sample air and therefore ~~; thus~~ $RFE_{H\&S}$ does not represent ambient ~~air~~conditions. In the ambient air, RH is larger and the AOPs ~~change~~ are different due to hygroscopic growth.

In addition to $RFE_{H\&S}$, we calculated a seasonal RFE by allowing the D to vary and by using more realistic seasonal values for A_C, and R_S. The seasonal variations of these parameters are presented in Fig. S1. ~~Here w~~We refer the seasonal RFE as RFE_S. The effect of ambient RH on ω_0 and b, and hence to RFE, was also studied. The seasonal RFE calculated for ambient RH is referred as $RFE_{S,moist}$. ~~More information about the seasonal D, A_C, R_S, and RH can be found in the supplementary material Sect. S2.~~

Seasonal A_C was derived by using ~~a~~ ceilometer data. The ceilometer was deployed at the Halli airport (about 25 km from SMEAR II) by Finnish Meteorological Institute (FMI) in 2010. The data were averaged for each month to get a seasonal variation. The lowest mean A_C was in July (~0.25) and the highest in January (~0.76).

For the seasonal R_S, reflectivity determined by Kuusinen et al. (2012) was used. They determined the R_S in a boreal forest for different amounts of canopy snow cover. According to the FMI, the average season of snow cover in Hyytiälä is from 16 November to 20 April (FMI: http://ilmatieteenlaitos.fi/lumitilastot, in Finnish only, last accessed: 13 March 2019) and for that time period we used $R_S = 0.314 \pm 0.14$ that Kuusinen et al. (2012) determined as the average albedo for a snow covered canopy. For snow-free forest we used $R_S = 0.126$, which is an average of the mean monthly albedos Kuusinen et al. (2012) determined for snow-free months.

In calculating the ω_0 and b ~~for~~ in ambient ~~air~~conditions, we used the equations ~~(Eqs. 1 and 2)~~ and parametrization presented in Sect. 2.3.1~~1~~ to convert the σ_{sca} and σ_{bsca} ~~for~~ to ambient RH; σ_{abs} was assumed to be constant with increasing RH, as Nessler et al. (2005) showed that the change in the σ_{abs} with increasing RH is very small compared to scattering. ~~There has not been measurements of hygroscopic growth parameters (q and γ) for σ_{bsca}, so we could not use the same parametrization in calculating the b to ambient RH. observed about 30 % decrease in b when the RH increased to 85 % at the Jungfraujoch measurement station. We used this observation as a linear approximation to estimate the how the b changes with varying RH. The estimated~~

~~b was then used in calculating the β for moist conditions.~~ The seasonally averaged RH was determined from RH measurements conducted at the height of 16 m. The lowest mean RH occurred in May (~62 %) and the highest in November (~95 %).

More information about the seasonal D, A_C, R_S, and RH can be found in the supplementary material Sect. S2.

~~The estimated uncertainties for the intensive AOPs are presented in Sect. S3 in the supplementary material. The uncertainties were calculated according to Sherman et al. (2015).~~

~~2.3.4 Data coverage~~

~~The trends and their significance were determined using the seasonal Kendall test described by . This test determines if there is a similar trend for each season (month) separately. All of the trends were calculated for the monthly medians, and at least 14 days of valid data in a given month were required for this month to be taken into account in the trend analysis.~~

~~If averaged over the whole measurement period, 81 % of the nephelometer data and 70 % of the aethalometer data were considered valid. All the AOPs had some gaps in the data (see Fig. 1). Monthly data coverage of σ_{sca} and σ_{abs} are presented in Table S1. Most of the gaps in the time series of AOPs during the summers of 2006 to 2010 were due to too high RH. The gap in 2010 was due to maintenance and installation of the dryers and the switching inlet system. Some additional σ_{bsca} data were missing, due to malfunction of the backscatter shutter of the integrating nephelometer. Dirty optics, malfunctions and maintenance caused the gaps in the σ_{abs} data in 2012 and 2015.~~

~~Until March 2010, the integrating nephelometer and the aethalometer measured sample air that was not dried with any external dryers. During winter, the relative humidity (RH) remained below 40 %, since the sample air warmed up to room temperature (about 22 °C). Sometimes in summer, the RH of the sample increased to over the 40 % limit. If the RH was above 40 %, the data were flagged as invalid and they were omitted from the data analysis if not stated otherwise. About 25 % of all the data before March 2010 had to be removed due to too high RH. Almost all of the removed data was from summer and fall months (June – October) and if regarding only these months, 46 % of the data were flagged. If the moist data was included the overall data coverage would increase to 89 % and 77 % for scattering and absorption data, respectively. After the installation of the Nafion dryers in March 2010, the humidity caused no further problems.~~

2.4.3 Properties calculated from particle size distribution~~s~~

~~With the s~~Size distributions were used~~, it is possible~~ to calculate differently weighted mean diameters. In this study, we used the geometric mean diameter (GMD) and the volume mean diameter (VMD). The GMD is the mean diameter that is weighted by the number concentration (N)

$$\mathrm{GMD} = \exp\left(\frac{\sum N_i \ln D_{p,i}}{\sum N_i}\right), \quad (15)$$

~~while~~ and the VMD is weighted by the particle volume (V)

$$\mathrm{VMD} = \frac{\sum D_{p,i} V_i}{V_{tot}} = \frac{\sum N_i D_{\mathrm{p},i}^4}{\sum N_i D_{\mathrm{p},i}^3}. \quad (16)$$

Since the particle number concentration is ~~focused~~ the highest ~~on~~for the nucleation and Aitken mode ~~sparticles~~, the GMD describes the distribution changes in the smallest sizes. The VMD, in contrast, is affected by the changes in the accumulation and coarse mode, since they contribute the most to the volume size distribution.

The measurements of the AOPs and size distribution can be combined ~~by determining~~to determine the complex refractive index ($m = n + ik$) that describes how much the particles scatter and absorb light. The m ~~and~~ can be used to model σ_{sca}, σ_{bsca} and σ_{abs} from the size distribution ~~measurements~~. ~~Index~~ The m consists of the real part (n), which accounts for the scattering, while the absorption is described by the imaginary part (k). Like ω_0, m provides information on the darkness and the chemical composition of the aerosol particles.

In this study, m was iterated from the σ_{sca}, σ_{abs} and size distribution measurements in a manner similar to that described by Virkkula et al. (2011). In the first step of the interpolation $\sigma_{sca,Mie}$ and $\sigma_{abs,Mie}$, which are the modeled scattering and absorption coefficients, were determined for the measured size distribution by using the Mie-theory with initial $m = 1.544 + 0.019i$. The ~~calculated~~ $\sigma_{sca,Mie}$ and $\sigma_{abs,Mie}$ were then compared with the measured σ_{sca} and σ_{abs}. If the calculated and measured values did not agree, the real part of m was first varied stepwise by 0.001 until the measured and modeled σ_{sca} agreed. Next, the imaginary part of m was varied in the same way until the measured and modeled σ_{abs} agreed. This iteration was continued until the measured and calculated values agreed within 1 %. The new imaginary part of m also affected σ_{sca} so the real part had to be reiterated. The MATLAB codes developed by (Mätzler, 2002) were used to model the Mie scattering and absorption.

2.4.4 Long-term trend analysis

Over the whole measurement period, 81 % of the nephelometer data and 70 % of the aethalometer data were considered valid. All of the AOPs had some gaps in the data (see Fig. 4). More detailed monthly data coverages of σ_{sca} and σ_{abs} are presented in Table S1. Most of the gaps in the time series of the AOPs during the summers of 2006 to 2010 were due to too high RH. If the moist data was included, the overall data coverage would increase to 89 % and 77 % for scattering and absorption data, respectively. After the installation of the Nafion-dryers in March 2010, the humidity caused no further problems. The gap in 2010 was due to maintenance and installation of the dryers and the switching inlet system. Some additional σ_{bsca} data were missing, due to malfunction of the backscatter shutter of the integrating nephelometer. Dirty optics, malfunctions and maintenance caused the gaps in the σ_{abs} data in 2012 and 2015.

All the months that had at least 14 days of valid data were included in the long-term trend analysis. The trends and their significance were determined using the seasonal Kendall test described by Gilbert (1987). This test determines if there is a similar trend for each season (month) separately. All of the trends were calculated for the monthly medians, and at least 14 days of valid data in a given month were required for this month to be taken into account in the trend analysis.

~~2.5 Trends~~

~~The trends and their significance were determined using the seasonal Kendall test described by Gilbert (1987). This test determines if there is a similar trend for each season (month) separately. All of the trends were calculated for the monthly medians, and at least 14 days of valid data in a given month were required for this month to be taken into account in the trend analysis.~~

3 Results and discussion

Below, we ~~first~~ present the descriptive statistics of the AOPs, their ~~trends, and~~ seasonal variations and long-term trends at SMEAR II. The figures of the AOPs in this section are presented in the green wavelength (550 nm for the scattering and intensive properties and 520 nm for the absorption measurements). In the figures of α_{sca} and α_{abs}, wavelength ranges of 450–700 nm and 370–950 nm were used. The results are presented for dry aerosols (RH < 40 %), if not stated otherwise.

3.1 ~~Overview of the data~~Characterization of boreal aerosol particles

The descriptive statistics of the AOPs of both the PM10 and PM1 particles are shown in Tables 1 and 2~~, respectively~~. The statistics are calculated from hourly data. Tables 1 and 2 show that for most of the variables the mean and the median values were quite different, which means that the data were not normally distributed. Therefore, we use the medians, which are not as sensitive to extreme values as the mean, to describe the characteristics of the AOPs.

~~From we see that the PM10 AOPs differ somewhat from the results of and that can be explained by the trends and by differences in the data processing. For example the mean σ_{sca} (~15 Mm^{-1}) at λ = 550 nm in this study was lower than that presented by (~18 Mm^{-1}) and by (~17 Mm^{-1}), which is probably due to the tendency of σ_{sca} to decrease (see Sect. 3.2). Another reason is that in the data processing Virkkula et al. (2011) used the earlier WMO/GAW recommendation and used data measured at RH < 50% and did not do any RH corrections. We also determined a strong tendency for σ_{abs} to decrease as well,~~

~~but the mean σ_{abs} (~2.1 Mm^{-1}, interpolated to 550 nm) was not much lower than the mean (~2.2 Mm^{-1}, at 550 nm) in the study by .This was due to the differences in the aethalometer data processing. reported no flow or spot size corrections and they used the algorithm of and C_{ref} = 3.688 at λ = 520 nm. Naturally, the different methods used in the absorption data processing also affected the optical properties that are dependent on the σ_{abs}, such as ω_0 and k. In the correction algorithm by , the C_{ref} is wavelength depended, which increases the α_{abs}. This was due to the differences in the aethalometer data processing. reported no flow or spot size corrections and they used the algorithm of and C_{ref} = 3.688 at λ = 520 nm. Naturally, the different methods used in the absorption data processing also affected the optical properties that are dependent on the σ_{abs}, such as ω_0 and k. In the correction algorithm by , the C_{ref} is wavelength depended, which increases the α_{abs}. reported a median α_{abs} = 1.4 that is notably higher than the median α_{abs} = 1.0 determined by our study. The difference in α_{abs} can be attributed to the correction algorithm since also in the present work the average and median α_{abs} = 1.36 and α_{abs} = 1.34 for the wavelength range 370–950 when the Arnott et al. (2005) algorithm is used. (see Table S2).~~

The median PM10 σ_{sca} and σ_{abs} at SMEAR II at green wavelength were 9.8 Mm^{-1} and 1.4 Mm^{-1}. In comparison to similar studies conducted at other Finnish measurement stations at Pallas in northern Finland (Lihavainen et al., 2015) and at Puijo tower in Kuopio, eastern Finland (Leskinen et al., 2012), results at SMEAR II showed the highest σ_{sca} and σ_{abs} ~~measured~~ for PM10 particles. At SMEAR II, the median σ_{sca} was about two times higher and σ_{abs} ~~about~~ more than three times higher than at Pallas, where the median ~~values of~~ σ_{sca} = 4.4~~7.9~~ Mm^{-1} and σ_{abs} = 0.4~~7~~ Mm^{-1} were measured at green wavelength. The Pallas station is remote, located 170 km north of the Arctic Circle, far from anthropogenic sources, which explains the low concentrations. At SMEAR II, σ_{sca} and σ_{abs} were about 1.4~~3~~ and 1.1~~1~~ times higher, than that measured at the Puijo tower, where the median ~~values~~ of σ_{sca} = ~~11.6~~7.2 Mm^{-1} and σ_{abs} = 1.0~~6~~ Mm^{-1} were measured at green and red wavelengths, respectively. Puijo tower is a semi-urban measurement station located only 2 km away from the Kuopio city center. At the Puijo tower, the measurements were conducted only on particles smaller than 2.5 µm, which explains part of the differences, at least for σ_{sca}.

Even though the σ_{sca} measured at SMEAR II is high compared to other measurements conducted in Finland, the air measured at SMEAR II is still clean when compared to ~~other European stations~~European sites. Due to the remote location, Pandolfi et al. (2018) observed ~~rather~~ lo~~w~~w σ_{sca} at SMEAR II compared to other European sites. Lower median σ_{sca} were~~as~~ observed only in the arctic region, at another Nordic rural station in Birkenes, Norway, and at several high mountain sites. ~~H~~The highest median σ_{sca} (> 40 Mm^{-1}) Pandolfi et al. (2018) observed in urban and regional sites in central and Eastern Europe.

~~The differences between the optical properties of the PM1 and PM10 particles are explained by the differences in concentrations, size distributions and chemical compositions. If only the PM10 data overlapping with the PM1 measurements were taken into account, the median values of σ_{sca}, σ_{abs}, ω_0, b, α_{sca}, α_{abs}, n, and k would have been 9.6 Mm^{-1}, 1.3 Mm^{-1}, 0.89, 0.14, 1.92, 0.97, 1.525 and 0.014 (σ_{sca}, ω_0, b, α_{sca}, n and k at 550 nm, σ_{abs} at 520 nm), respectively. The extensive variables (σ_{sca}, σ_{bsca} and σ_{abs}) were smaller for the PM1 measurements, since there was less particle volume interacting with the radiation.~~

~~The α_{sca} and b are related to the sizes of the particles, so they were naturally different between the PM1 and PM10 particles. For the smaller PM1 particles, the α_{sca} and b were larger than for the PM10 particles. However, b does not have as large a difference between the PM1 and PM10 particles as α_{sca}.~~

From Table 1 we see that the PM10 AOPs differ somewhat from the results of Virkkula et al. (2011) and Pandolfi et al. (2018) that can be explained by the trends and by differences in the data processing. For example the median σ_{sca} (~10 Mm^{-1}) at λ = 550 nm in this study was lower than that presented by Virkkula et al. (2011) (~12 Mm^{-1}) and by Pandolfi et al. (2018) (~11 Mm^{-1}), which is probably due to the tendency of σ_{sca} to decrease (see Sect. 3.2). Another reason is that in the data processing Virkkula et al. (2011) used the earlier WMO/GAW recommendation (WMO/GAW, 2003) and used data measured at RH < 50% and did not do any RH corrections.

We also determined a strong tendency for σ_{abs} to decrease as well and the median σ_{abs} (~1.3 Mm^{-1}, interpolated to 550 nm) was somewhat lower than the median (~1.5 Mm^{-1}, at 550 nm) in the study by Virkkula et al. (2011). However, the σ_{abs} between these two studies are not fully comparable due to the differences in the aethalometer data-processing. Virkkula et al. (2011) reported no flow or spot size corrections and they used the algorithm of Arnott et al. (2005) and C_{ref} = 3.688 at λ = 520 nm. Naturally, the different methods used in the absorption data processing also affected the optical properties that are dependent on the σ_{abs}, such as ω_0 and k. In the correction algorithm by Arnott et al. (2005), the C_{ref} is wavelength depended, which increases the α_{abs}. Virkkula et al. (2011) reported a median α_{abs} = 1.4 that is notably higher than the median α_{abs} = 1.0 determined by our study. The difference in α_{abs} is attributed to the correction algorithm since also in the present work and median α_{abs} = 1.34 for the wavelength range 370–950 when the Arnott et al. (2005) algorithm is used. (see Table S2).

The differences between the AOPs of the PM1 and PM10 particles are explained by the differences in concentrations, size distributions and chemical compositions. If only the PM10 data overlapping with the PM1 measurements were taken into account, the median PM10 σ_{sca}, σ_{abs}, ω_0, b, α_{sca}, α_{abs}, n, and k would have been 9.6 Mm^{-1}, 1.3 Mm^{-1}, 0.89, 0.14, 1.92, 0.97, 1.525 and 0.014 (σ_{sca}, ω_0, b, α_{sca}, n and k at 550 nm, σ_{abs} at 520 nm). For PM1 the medians were 7.1 Mm^{-1}, 1.2 Mm^{-1}, 0.87, 0.15, 2.41, 1.03, 1.487 and 0.021, respectively. The extensive variables (σ_{sca}, σ_{bsca} and σ_{abs}) were smaller for the PM1 measurements, since there was less particle volume interacting with the radiation. The α_{sca} and b are related to the sizes of the particles, so they were naturally different between the PM1 and PM10 particles. For the smaller PM1 particles, the α_{sca} and b were larger than for the PM10 particles. However, b does not have as large a difference between the PM1 and PM10 particles as α_{sca}.

On average submicron particles caused about 75 % of the total scattering of the PM10 particles. This was apparently a lower fraction than in the previous analysis of SMEAR II scattering data. Virkkula et al. (2011) stated that the average contributions of submicron particles to the total σ_{sca} was in the range of 88–92 %, clearly more than in the present work. However, in that study the scattering size distribution and the contributions of the various size ranges were calculated from particle number size

distributions with a Mie model and the physical diameters (D_p) were used whereas here the PM1 corresponds to particles smaller than the aerodynamic diameter D_a of 1 µm. With particle density of 1.7 g cm^{-3} this corresponds to the physical diameter $D_p = (1/1.7)^{½}$ 1 µm ≈ 0.77 µm. The contribution of particles smaller than 0.77 µm is approximately 85 % if it is estimated from Fig. 11 of Virkkula et al. (2011), still more than the ~75 % contribution of submicron scattering shown here. This may have resulted from the cutoff diameter of the PM1 impactor is not exactly sharp and also that the particles entering the impactor may have still been somewhat moist and thus larger than their dry size and were therefore removed from the sample stream. Further analysis of the difference is omitted here.

The PM1 particles absorbed about 90 % of the total PM10 particle absorption. So for the σ_{abs} there were no large difference in the σ_{abs} of the PM1 and PM10 particles. The coarse mode particles are typically primary and they have a quite high ω_0 so their absorption is minor compared with the PM1 particles. The soot particles, which account for most of the particulate absorption, are typically submicron particles. Due to the relative differences in the scattering and absorption, ~~in~~ the median ω_0 and n were lower for~~,~~ the PM1 particles than PM10 particles.

~~absorbed more light relative to scattering than the PM10 particles. The α_{sca} and b are related to the sizes of the particles, so they were naturally different between the PM1 and PM10 particles. For the smaller PM1 particles, the α_{sca} and b were larger than for the PM10 particles. However, b does not have as large a difference between the PM1 and PM10 particles as α_{sca}.~~

~~The average values of the PM10 particles given in Table 1 are calculated by excluding the periods when the RH > 40 %. If these periods of σ_{sca} and σ_{abs} measurements were included in the analysis and the moist scattering data were corrected to dry conditions by using the Eqs. 1 and 2, we would get median values of σ_{sca} = 10.3 Mm^{-1}, σ_{abs} = 1.5 Mm^{-1}, ω_0 = 0.88, b = 0.15, α_{sca} = 1.91, α_{abs} = 0.98, and RFE$_{H\&S}$ = 23 for PM10 (σ_{sca}, ω_0, b, and RFE$_{H\&S}$ at 550 nm, σ_{abs} at 520 nm, α_{abs} at 370 nm/950 nm and α_{sca} at 450 nm/700 nm). The differences are not large compared to values presented in Table 1, so omitting the moist data periods from the data set does not seem have a large effect on the median AOPs in this data set~~

3.41.1 Seasonality of AOPs ~~variation~~

The seasonal variation in the PM10 AOPs was clearly visible in the 11.5~~2~~-year record shown in Fig. ~~5~~1. The seasonal variations in σ_{sca} and σ_{bsca} (Figs. 1~~5~~a and b) were~~as~~ not yet as clear in Virkkula et al. (2011) as it is now. For the σ_{sca} and σ_{bsca}, two local maxima occurred during late winter (February) and late summer (July). The local minima occurred during spring (April) and late autumn (October). The σ_{abs} showed the highest values during winter (February) and the lowest values during summer (June). Part of this variation is explained by boundary layer dynamics. In summer, the boundary layer is higher and well mixed, therefore ~~thus~~ diluting the aerosol concentration and~~.~~ ~~I~~in winter the situation is the opposite and the pollution accumulates in the shallow boundary layer. Also, the sources of aerosol particles vary seasonally, which affects the seasonal concentration.

For the extensive properties, the highest values occurred at the same time in winter (February) when the ω_0 was also low, which ~~means~~indicates that there were larger amounts of particles from anthropogenic sources than in summer. Hyvärinen et al. (2011) observed increased equivalent black carbon (eBC, meaning- optically measured BC) concentrations at SMEAR II in winter, when the long-range transport brings pollution from the central and ~~eastern~~Eastern Europe. However, Hienola et al. (2013) estimated that about 70 % of the measured eBC at SMEAR II is emitted from local or regional sources or transported from Finnish cities, so also the local and regional emissions have a significant role in the elevated eBC concentrations. Since February is one of the coldest months in Finland, domestic wood burning in the local and regional area increases the particle concentration (Karvosenoja et al., 2011). Pollution can also be transported from nearby cities (the largest and closest are Tampere and Jyväskylä). Hyvärinen et al. (2011) observed no remarkable changes in the Hyytiälä eBC concentrations coming from the Tampere region. However, the largest concentrations they observed came from the direction of Orivesi, a small town (population about 9 000) 20 km from the measurement station.

~~In summer, the ω_0 had its highest values since the σ_{sca} was high and the σ_{abs} was low. In summer, the anthropogenic influence is not as strong as in the winter since the energy consumption is lower. The contribution of particles from natural sources increased during spring and summer when the vegetation was active and growing. The seasonal variation in the n and k was clearly associated with the ω_0. In summer when the ω_0 was high, n was high and k was low. In winter, the relationship was the opposite. The scattering maximum in summer was probably caused by secondary organic particles explaining why the b and α_{sca} are also maximal.~~

The ~~There is an anti-correlation between the seasonal variations of ω_0 and α_{abs}. α_{abs}~~ is typically associated with the source of the BC and it is often used to quantify whether the BC is traffic or wood burning related (Sandradewi et al., 2008; Zotter et al., 2017) so that high α_{abs} is a sign of wood burning. In the source apportionment, α_{abs} close to one indicates that the BC is from traffic-related sources. Since we observed relatively higher α_{abs} in winter, the results are in line with the assumption of domestic wood burning that takes place during winter. However, in summer, α_{abs} was often < 1, which would yield an unphysical fraction (over a 100 %) of traffic related BC. Values below one could have been caused by large BC particles (D_p > 100 nm) that have a purely scattering coating (Lack and Cappa, 2010). It must be noted that the α_{abs} depends also on the correction algorithm. For example, if the σ_{abs} was corrected with the algorithm proposed by Arnott et al. (2005), the median of α_{abs} would have been 1.34 ± 0.51 (see Table S2). Using the α_{abs}, which was determined by using the correction by Arnott et al. (2005), the results for the source apportionment would be different and they would show higher fraction of BC from wood burning.

The ~~maximum values of α_{abs}~~ is also used to describe the chemical properties of the particles. ~~(> 1) occur in winter, which means that light is absorbed more efficiently at shorter wavelengths than in summer.~~H~~-A h~~igher α_{abs} ~~may sugges~~indicates~~t~~ that light is absorbed not only by BC, but also by some light-absorbing organic carbon compounds, i.e. brown carbon (BrC). In using only α_{abs}, it is difficult to determine if the particles consist of BrC, since BC particles with coating can also have an α_{abs}

up to 1.6 (Lack and Cappa, 2010). In Fig. 1g5 we can see that the value of 1.6 is not really reached at SMEAR II if the correction algorithm by Collaud Coen et al. (2010) was used. Since α_{abs} is dependent on the size of the BC core, the thickness of the coating and the *m* of the coating, ~~more detailed investigation would be needed to determine why α_{abs} is varies.~~further investigation of its complex nature is omitted here.

~~Also, the α_{abs} is typically associated with the source of the BC and it is often used to quantify whether the BC is traffic or wood burning related so that high α_{abs} is a sign of wood burning. In the source apportionment, α_{abs} close to one indicates that the BC is sourced from traffic. Since we observed relatively higher α_{abs} in winter, the results are in line with the assumption of domestic wood burning that takes place during winter. However, in summer, α_{abs} was often < 1, which would yield an unphysical fraction (over a 100 %) of traffic related BC. Values below 1 could have been caused by large BC particles (D_p > 100 nm) that have a purely scattering coating . It must be noted that the α_{abs} depends also on the correction algorithm. For example, if the σ_{abs} was corrected with the algorithm proposed by , the mean ± SD of α_{abs} would have been 1.36 ± 0.51 (see Table S2). Using the α_{abs}, which was determined by using the correction by , the results for the source apportionment would be different and they would show higher fraction of BC from wood burning. Further investigation of the complex nature of α_{abs} is omitted here.~~

In summer, the ω_0 had its highest values since the σ_{sca} was high and the σ_{abs} was low. High σ_{sca} but low σ_{abs} suggests that the anthropogenic influence was not strong in summer and that there was higher contribution of particles from natural sources when the vegetation was active and growing. The scattering maximum in summer was probably caused by secondary organic particles (Tunved et al., 2006).

The seasonal variation in α_{sca} and *b* depends on the seasonal variation in the size distribution of the particles. Both α_{sca} and *b* were maximal in summer and minimal in winter, suggesting that in summer, the particle population consisted of smaller particles than in winter. A trajectory analysis by Virkkula et al. (2011) showed that the highest α_{sca} were originated within a ~200 km radius around the station, which means that the smallest particles were rather freshly emitted. This supports the hypothesis that in summer a high fraction of the aerosols are secondary organic particles.

The impact of smaller particles in summer, indicated by the high α_{sca} and *b*, is seen also in Fig. 2a, which presents the seasonal variation of the σ_{sca} PM1/PM10 ratio. The ratio describes the fraction of fine particles (PM1) on the PM10 σ_{sca} and it shows that, in addition to summer, the fine particles have a high impact also in winter, which was not seen in α_{sca} and *b* variation. Closer investigation on the seasonally averaged size distributions, which areis presented in Fig. S63 (and S7), revealsthat the seasonal variations of α_{sca} and *b* are more depended on the shifts in the accumulation mode than in the coarse mode. Fig. 3 shows that iin winter, the VMD_{tot} hadwas experiencing its minimum due to a lack of coarse mode particles.~~(Schumacher et al., 2013).~~ This is in contrast with the observation ofr smaller α_{sca} and *b*, but it supports the maximum we see in the σ_{sca} PM1/PM10 ratio. ~~In fact, t~~The seasonal variations of α_{sca} and *b* wasere then explained by the seasonal variation of volumetric mean diameter calculated for particles smaller than 1 µm (~~accumulation mode and~~ VMD_{fine}). ~~, which~~VMD_{fine} is a good indicator for the

shifting accumulation mode and it is not affected by the coarse mode. In winter, when the α_{sca} and b were small, the accumulation mode was shifted towards larger sizes and the median of VMD_{fine} was about 350 nm. In summer, when the α_{sca} and b had their maxima, the situation was the opposite and VMD_{fine} was smaller, about 250 nm.~~Virkkula et al. (2011)~~

~~3.5 Variation between the PM10 and PM1 measurements~~

~~Even though the average values between the optical properties of the PM10 and PM1 particles differed, their seasonal variation was similar for all the various properties. However, there was a seasonal variation in the relationship between the PM10 and PM1 extensive properties, as shown in Fig. 6. The seasonal variation in the PM1/PM10 ratio describes the impact of the coarse and fine particles on the σ_{sca} and σ_{abs}.~~

~~For the σ_{sca} the seasonal variation in the PM1/PM10 ratio was clear, but for the σ_{abs} there seemed to be no seasonal variation in the ratio whatsoever. The seasonal medians of the PM1/PM10 ration for the σ_{sca} varied from 0.7 to 0.8, and on average submicron particles caused about 75 % of the total scattering of the PM10 particles. This was apparently a lower fraction than in the previous analysis of SMEAR II scattering data. stated that the seasonal average contributions of submicron particles to the total σ_{sca} was in the range of 88–92 %, clearly more than in the present work. However, in that study the scattering size distribution and the contributions of the various size ranges were calculated from particle number size distributions with a Mie model and the physical diameters (D_p) were used whereas here the PM1 corresponds to particles smaller than the aerodynamic diameter D_a of 1 µm. With particle density of 1.7 g cm^{-3} this corresponds to the physical diameter $D_p = (1/1.7)^{½}$ 1 µm ≈ 0.77 µm. The contribution of particles smaller than 0.77 µm is approximately 85 % if it is estimated from Fig. 11 of , still more than the ~75 % contribution of submicron scattering shown here. This may have resulted from the cutoff diameter of the PM1 impactor is not exactly sharp and also that the particles entering the impactor may have still been somewhat moist and thus larger than their dry size and were therefore removed from the sample stream. Further analysis of the difference is omitted here.~~

~~The maxima of the submicron particle scattering occurred in winter and summer. The summer peak coincided with the maxima of the PM10 α_{sca}, which already indicates that smaller particles play a major role in the size distribution. However, this correlation between the PM1/PM10 ratio and α_{sca} was not observed in winter. In Fig. 2 (and in Fig. S7), it can be seen that the VMD_{tot} always decreased in the wintertime indicating also the lack of coarse particles. However, on average, the accumulation mode is relatively large compared to the coarse mode and it is shifted towards the larger diameters. This is presented in the supplementary material (Figs. S6 and S7). The large accumulation mode caused α_{sca} to be low, even though there was relatively less scattering by the coarse particles.~~

The seasonal variation in the size distribution did not affect the σ_{abs} PM1/PM10 ratio and ~~For the σ_{abs}, the~~the median of the PM1/PM10 ratio did not ~~greatly~~ vary seasonally. However, ~~. The PM1 particles absorbed about 90 % of the total PM10 particle absorption. So for the σ_{abs} there were no large difference in the σ_{abs} of the PM1 and PM10 particles. The coarse mode particles are typically primary and they have a quite high ω_0 so their absorption is minor compared with the PM1 particles. The soot particles, which account for most of the particulate absorption, are typically submicron particles.~~

~~Th~~ the deviation of the σ_{abs} PM1/PM10 ratio had a clear~~ly~~ seasonal varie~~d seasonally~~ation. In summer, the variation was considerably higher than in winter. In the correction algorithm, which was used for the absorption data (Eq. 1~~3~~), part of the σ_{sca} is subtracted from σ_{abs} as an apparent absorption (Muller et al., 2011). The~~is~~ subtraction of σ_{sca} causes relatively high uncertainty when the σ_{abs} is low and σ_{sca} is high, like it is in summer. This uncertainty is emphasized for PM10 measurements, since the σ_{sca} is relatively higher than σ_{abs}, if compared to PM1 measurements. The uncertainty in the measurements also explains why ~~there were so~~ many values were above ~~1~~ one ~~measured~~ in the PM1/PM10 σ_{abs} ratio.

~~The evolution of the PM1/PM10 ratios were also investigated but we observed no statistically significant trends for either σ_{sca} or σ_{abs}.~~

3.2 Long-term trends of the AOPs~~Trends~~

The about 11.5-year-long time series of the PM10 ~~and PM1~~ AOPs were used to determine ~~the~~long-term trends ~~trends for the optical properties~~. For a comparison, we also conducted the trend analysis for the PM1 data, which ~~the PM10 trend analysis we used data from about 10.5 years and for the PM1 trend analysis we used~~had shorter, about 7.5 ~~-~~year ~~s~~ long, time series. It must be noted that trends for shorter time series are more sensitive to the year-to-year variability and must be interpreted with caution. The slopes of the trends and the trend statistics are presented in Table 3. The table also presents the trends as percentages, which were calculated by dividing the slope by the overall median value of the variable. The trends are also plotted in Fig. 4~~1~~, where the monthly medians of the PM10 AOPs at SMEAR II used in this analysis are presented. The monthly medians are included in Fig. 4~~1~~ only if the month had at least 14 days of valid data.

In all the extensive properties, the trends were negative. The slopes of the trends for PM10 σ_{sca}, σ_{bsca} and σ_{abs} were -0.32, -0.038, and -0.086 $Mm^{-1}yr^{-1}$, respectively. The decrease in the extensive properties were due to decrease in the total particle number concentration (N_{tot}) and total volume of the particles (V_{tot}) that can be seen in the combined TDMPS and APS data presented in Figs. 2~~5~~a and ~~band~~ in Table 3. The relative decrease in V_{tot} (-4 $\%yr^{-1}$) was rather similar to that of σ_{sca} (-3 $\%yr^{-1}$). Also, Pandolfi et al. (2018) showed a statistically significant trend for σ_{sca} (-0.588 $Mm^{-1}yr^{-1}$) measured at SMEAR II. They reported negative trends at other European sites as well and they determined that the average decrease was about -35 % for a

ten-year period, which is a bit larger reduction than that observed at SMEAR II (-30 % for a ten-year period). The results are in line with the decrease in particle number concentration observed in European countries (Asmi et al., 2013). Also the remotely measured decreasing trend for aerosol optical depth (δ) supports the decreasing trends in Europe (Li et al., 2014). Decreasing trends for σ_{sca} are not only observed in Europe; Collaud Coen et al. (2013) and Sherman et al. (2015) reported negative trends for σ_{sca} in North America as well.

The observed relative decrease in σ_{abs} (-6 %~~-~~yr^{-1}) was about twice as large ~~than~~as that of σ_{sca} (-3 %yr^{-1}). The differences in the trends indicates that during the measurement period, the amount of absorbing material, such as BC and BrC, decreased relatively faster than the amount of scattering material (e.g~~q~~. sulfate). It is also possible that the decrease in non-absorbing compounds decreased the σ_{abs} since a non-absorbing coating around an absorbing particle can act as a lens, which increases absorption. The study by Collaud Coen et al. (2013), which included also σ_{abs} data, observed negative trends for both σ_{sca} and σ_{abs} at the Bondville measurement station in Illinois, USA, but~~.~~ ~~T~~there the trends of both σ_{sca} and σ_{abs} were ~~similar in magnitude (~~about -3 %yr^{-1}~~)~~. Sherman et al. (2015) did not observe this decreasing trend in σ_{abs} ~~trend~~ later.

~~For the PM1 σ_{abs}, we observed a very steep decrease (-12 %yr^{-1}), which was probably caused by very high σ_{abs} measured in January and February in 2012. Also, the data gaps in winter 2013 and 2015 could have affected the trends. The time series, of which the trends were determined for the PM1 measurements, were only 7.5 years long. Trends, which are determined for shorter time series are more sensitive to year-to-year variability. This kind of extreme values can induce relatively large trends, which is why trend analysis for short time series (less than ten years) should be treated with caution.~~

Since the aerosol particles were absorbing less light than before, there was a tendency for the ω_0 to increase. As shown by the increase in ω_0 and the decrease in the extensive properties, the air measured at SMEAR II was less polluted than before. ~~The h~~Higher ω_0 indicates that the measurements were less affected by particles produced by traffic emissions or incomplete combustion. Li et al. (2014) reported mostly positive trends for ω_0 ~~tha,t~~ which were determined by remote measurements conducted in Europe. The decreasing trend for k supports the tendency for ω_0 to increase, since the negative trend for the imaginary part of m means that ~~particles~~ particulate matter absorbs less light. The α_{abs} and n,~~-~~ which are~~is~~ also related to the chemical composition of the particles, showed no significant trends ~~for either the PM1 or PM10 particles. The negative trend for the interpolated n was only significant for the PM1 particles. The tendency for the interpolated n to decrease could have been caused by changes in the chemical composition.~~

~~The trends of the b and α_{sca} were also investigated.~~ The~~ese~~ trend of b and α_{sca} ~~s~~ describe how the size distribution of the aerosol particles has changed. For the PM10 b and α_{sca} the trends were positive, but for the ~~PM10~~ α_{sca} however, the p value was 0.07, so there was only a weak evidence for the positive trend in ~~PM10~~ α_{sca}. ~~For the PM1 the trends for both, b and α_{sca}, were positive and statistically significant.~~ Increasing b ~~and α_{sca}~~ indicates that ~~the mean size of~~ the size distribution ~~was moving~~moved towards

smaller particles. This hypothesis was investigated by conducting the trend analysis for the volumetric and geometric mean diameters of particles smaller than 10 µm (VMD_{tot} and GMD_{tot}), which were calculated from the size distribution. The results are presented in Table 3. We did not observe significant trend for the GMD_{tot}, which is sensitive to the smallest particles of the size distribution. However, a statistically significant trend was observed for VMD_{tot} (Fig. 5c), which depends on the accumulation and coarse mode particles and therefore correlates better with the extensive AOPs than the GMD (Virkkula et al., 2011). Decreasing VMD_{tot} indicates ~~The~~a shift ~~of~~ in the size distribution towards smaller diameters ~~is also observed in the negative trend of the volume mean diameter (VMD_{tot}), presented in Fig. 2c and in Table 3,~~ supporting the increasinge ~~in~~ *b* and α_{sca}.

In addition to SMEAR II, ~~Also,~~ Pandolfi et al. (2018) observed significant increasing trends for *b* at ~~SMEAR II and other~~several European stations. ~~For the α_{sca}, however, they observed both positive and negative trends at different stations.~~SMEAR II they observed significant increasing trend also for α_{sca}, which was determined by using the wavelength range of 550–700 nm. At other sites, they observed mostly decreasing trends. Pandolfi et al. (2018) suspected that the variation was caused by differing trends of the coarse and accumulation mode particle concentration. Also Li et al. (2014) observed negative trends for the α_{sca} across the Europe and they suggested the trends were caused by a decrease in fine particle emissions.

~~Since the trends of *b* and α_{sca} for the PM10 and PM1 measurements were similar, the trends in α_{sca} and *b* may indicate that the concentration of larger particles in the accumulation mode was decreasing, since a decrease in coarse particle concentration only could not cause the decreasing trend of PM1 α_{sca}. The changes in the size distribution were investigated by determining a trend for each TDMPS and APS measurement channels.~~

As a comparison, we also conducted the trend analysis for the PM1 measurements, even though there was only 7.5-years-long time series available. The trends observed for the PM1 particles were similar to those of PM10: decreasing trends for the extensive properties and increasing trends for the ω_0 and *b*. For the PM1, the trends for both, *b* and α_{sca}, were positive and statistically significant. This observation suggests that especially the concentration of larger particles in the accumulation mode was decreasing, since a decrease in coarse particle concentration only could not cause the decreasing trend of PM1 α_{sca} nor *b*. A closer look in the size distribution, which is presented in Sect. S6, pointed out that relatively greatest decrease occurred for accumulation mode particles that were 500–800 nm in diameter. On average, the volume size distribution of accumulation mode particles peaks around 300 nm (see Fig. 3) so the greatest decrease occurred at the larger sizes of the accumulation mode.

The decrease in the larger side of the accumulation mode might be caused by a decrease in long-range transported pollution. Aged pollution particles might be grown by other substances, such as SO_2 in the atmosphere so their sizes are larger than freshly emitted or formed particles. SO_2, emissions have decreased in Europe (Tørseth et al., 2012), which supports this assumption. A trajectory analysis by Virkkula et al. (2011) showed that α_{sca} was clearly higher in air masses from continental

Europe than from the North Atlantic but also that the highest α_{sca} values were measured in air masses sources from within southern Finland, which would suggest that larger particles are not from nearby the station.

The installation of the Nafion-dryers in 2010 could have caused an artificial decrease in ~~σ_{sca} or σ_{abs}~~the AOPs since the dryers increase the deposition of the particles and may decrease the sizes of hygroscopic particles. However, the similar trend between the PM1 and PM10 AOPs does not support this suspicion, since d~~s were similar for the PM10 and PM1 particles. D~~uring the PM1 measurements, there were no large changes in the measurement line, so the observed trends were probably not caused by any technical ~~changes~~ issues in the measurement line.

~~A lot of summer time data measured before 2010, were marked invalid due to too high humidity and it could have affected the trend analysis. To test this hypothesis, we used Eqs. 1 and 2 to correct the σ_{sca} to dry conditions and included this data in the trend analysis. The σ_{bsca} was not corrected to dry conditions. Also, moist (RH > 40 %) absorption data was included in this test. Including the originally omitted data in the trend analysis, we observed statistically significant (p value < 0.05) trends for the PM10 σ_{sca}, σ_{abs}, ω_0, and RFE with the slopes of -4 % yr^{-1}, -5 % yr^{-1}, 0.2 % yr^{-1}, and 0.5 % yr^{-1} respectively. Still, there were decreasing trends for extensive properties and positive trends for ω_0. However the difference between the σ_{sca} and σ_{abs} trends decreased from 3 % to 1 % if compared against the trends that were determined only for the dry conditions. Including the moist data and acquiring longer data sets in the trend analysis suggests that the relative difference between the trends of σ_{sca} and σ_{abs} might not be that large. Not correcting the σ_{bsca} to dry conditions probably explains why we do not see a significant trend for the b here.~~

In addition to the general trends, we also investigated how the trends of σ_{sca} and σ_{abs} varied between ~~different~~ the seasons. In this analysis, the periods of RH > 40 % were included ~~(σ_{sca} corrected to dry conditions according to Eqs. 1 and 2)~~ in order to avoid the data gaps in summer and autumn before 2010 and to have time series with equal lengths for each season. The moist σ_{sca} was estimated to dry conditions according to Eqs. 1 and 2. ~~.~~The trends were determined separately for spring (March, April, May), summer (June, July, August), autumn (September, October, November), and winter (December, January, February). The trend calculations were conducted by using the monthly medians (see timeseries in Fig. S3) and t~~. T~~he results are presented in Table 4.

Table 4 shows that σ_{sca} and σ_{abs} had a decreasing trend for each season, but ~~for~~ in the autumn the trends were not significant. Both σ_{sca} and σ_{abs} experience the fastest absolute decrease in winter when the energy consumption is the highest and pollution sources are more pronounced; on the opposite, the trends ~~are~~ were the least negative in summer when there is less pollution. In spring, the absolute trends were less negative than compared to winter. ~~However, for the σ_{abs}, we observed that the relative trend in spring (-9 %yr^{-1}) was steeper than in winter (-8 %yr^{-1}).~~

~~3.3 Aerosol optical properties and size distribution~~

~~To obtain a better view on how the shape of the size distribution affected the AOPs, the various AOPs were compared against the GMD and VMD. The results of the comparison are shown in Fig. 3. The GMD was mostly affected by the small nucleation and Aitken mode particles, which are high in number concentration; the accumulation mode particles also had some effect on the GMD. Since only the smallest particles affect the GMD it is practically the same for the fine (D_p < 1 µm) and total (D_p < 10 µm) particle size distribution. Thus, we present the comparison of GMD and AOPs only for the PM10 particles (Figs. 3a – d). The VMD, however, was heavily affected by the size distribution of the accumulation and coarse mode particles, since they predominated in the particle volume size distribution. This explains why there was notable differences for the PM10 (Figs. 3e – h) and PM1 (Figs. 3i – l) particles, when their AOPs were compared against the VMD calculated for particles smaller than 10 µm (VMD_{tot}) and VMD calculated for particles smaller than 1 µm (VMD_{fine}), respectively.~~

~~The σ_{sca} correlated positively with the GMD due to the changes in particle concentration in the accumulation mode. The median number and volume size distribution for situations when GMD was below 50 nm or above 100 nm are presented in Fig. 4c. There was a clear difference in the number and volume size distribution in the accumulation mode when the GMD limit was varied. From the number size distribution, it can be seen that GMD increased due to a larger accumulation mode and lack of particles in the nucleation and Aitken modes. Nucleation and Aitken mode particles are mainly produced and grown by condensing vapors and since larger particles in the accumulation mode act as a condensation sink for vapors, the smaller particle modes do not tend to exist when accumulation mode particles are present.~~

~~For the PM10 particles, there was a negative correlation between the σ_{sca} and VMD, but when the coarse particles were ignored, i.e. for PM1 particles, the correlation became positive. The negative correlation for the PM10 particles is caused by the changes in the accumulation and coarse mode particle concentration. This is shown in further detail in Fig. 4a, where the median volume size distribution is presented for situations in which the VMD_{tot} > 1500 nm, 500 nm < VMD_{tot} < 1000 nm and VMD_{tot} < 500 nm. When the VMD_{tot} was high, there was a strong coarse mode but the accumulation mode was clearly smaller than in the other situations. Even though the VMD_{tot} was high, the lack of accumulation mode particles decreased the scattering. From Fig. 3a, it can be seen that the σ_{sca} became maximal when the VMD_{tot} was about 500–1000 nm. In this VMD range, the coarse mode was slightly smaller but the accumulation mode clearly increased, thus increasing the scattering. When the VMD_{tot} < 500 nm, the coarse mode was almost completely missing that caused the σ_{sca} to decrease, even though there was a large accumulation mode present.~~

~~estimated that fresh eBC particles observed at SMEAR II are in the size range of 80 – 120 nm. That estimate was calculated in a simplified way from the relationship between particle number concentrations and BCe concentrations. A better estimate is obtained from the size dependence of ω_o. The darkest aerosol has ω_o < 0.6 and GMD in the range of about 30 – 70 nm~~

(Fig. 3b, 3f, and 3j). This has been shown to be the range of fresh BC (e.g., Kittelson, 1998; Casati et al., 2007; Zhang et al., 2008) which suggests the source of BC is not far, probably within some kilometers only.

The size dependent properties α_{sca} and b for PM10 acted rather differently when compared with the GMD and VMD_{tot}. The α_{sca} increased with growing GMD (Fig. 3c), which is in contrast with the expectation that the α_{sca} would decrease when the size distribution is dominated by larger particles. The observation that the α_{sca} increased with an increasing GMD is in line with the analyses made for AOPs and size distributions measured in Guangzhou, China by , at SMEAR II by , and in Nanjing, China by . To study the reasons behind this relationship we generated first unimodal size distributions with two geometric standard deviations GSD = 1.5 and 2.0 and calculated both σ_{sca} and σ_{bsca} at λ = 450, 550, and 700 nm with the Mie code with m = 1.517 + 0.19i and the α_{sca} and b from them. For unimodal size distributions the α_{sca} decrease with increasing GMD as is shown by the lines in Fig. 3c. showed that the relationship may be the opposite for bimodal size distributions. explained this behavior by that adding a larger or coarse particle size mode to a fine particle mode that is inefficiently scattering – for instance nucleation and Aitken mode particles – the larger mode contributes more efficiently to the Ångström exponent than the fine mode. The contribution of the particles smaller than 100 nm to GMD is larger than that of the larger particle modes, which leads to the observed relationship. To study this in more detail we generated also bimodal size distributions. The analysis presented in the supplement (S6) shows that the α_{sca} of bimodal size distributions can be calculated as a linear combination of the α_{sca} of the modes, weighted by the fractions of σ_{sca} of the respective modes. This explains the increase of α_{sca} with growing GMD.

In addition, at SMEAR II the size distribution typically consists of not only two but multiple modes that explains the observed relationship. An additional qualitative analysis of this relationship is given in Fig. 4c, where the median number and volume size distributions are plotted for situations in which the GMD was < 50 nm and > 100 nm. By comparing these two situations, it can be seen that when the GMD > 100 nm the accumulation mode was much larger than when GMD < 50 nm. Since the coarse mode is rather similar for both cases, the α_{sca} varied due to changes in the accumulation mode. For the α_{sca} and VMD, the correlation was negative (Fig. 3g) that supports the expectations. However, the α_{sca} measured for the PM10 particles was much higher than that modeled for the unimodal distributions, which can also be explained by the multiple modes of the real size distributions.

There was a negative correlation between the GMD and PM10 b (Fig. 3d) as expected, but the correlation was rather weak. On the contrary, the correlation between the VMD_{tot} and PM10 b was slightly positive (Fig. 3h). The negative correlation of α_{sca} with VMD_{tot} and the positive correlation of b with VMD_{tot} for the PM10 particles indicates that the α_{sca} and b were sensitive to different size ranges. The α_{sca} decreased when there are more coarse particles present, but for the b the coarse particles seem to have no expected effect and the b increased with increasing VMD_{tot}. Fig. 4a. shows that when the VMD > 1500 nm, the peak of $dV/d\log D_p$ in the accumulation mode was much lower and tilted towards the smaller diameters than compared to the

situations where the VMD < 1000 nm. This is in line with , who stated that in the Jungfraujoch data, *b* was sensitive to particles smaller than 400 nm and that the sensitivity of the α_{sca} was at its maxima for particle diameters between 500 and 800 nm.

For the PM1 particles, the measured α_{sca} and *b* were well in line with the modeled values (Figs. 3k and l), since the coarse mode particles were removed prior to the measurements, the shape of the size distribution was closer to a unimodal size distribution, and the VMD_{fine} described better how the accumulation mode shifted.

For the PM1 σ_{abs}, we observed a very steep decrease (12 %yr^{-1}), which was probably caused by very high σ_{abs} measured in January and February in 2012. Also, the data gaps in winter 2013 and 2015 could have affected the trends. The time series, of which the trends were determined for the PM1 measurements, were only 7.5 years long. Trends, which are determined for shorter time series are more sensitive to year-to-year variability. This kind of extreme values can induce relatively large trends, which is why trend analysis for short time series (less than ten years) should be treated with caution.

3.4 Seasonal variation

The seasonal variation in the PM10 AOPs was clearly visible in the 12-year record shown in Fig. 5. The seasonal variation in σ_{sca} and σ_{bsca} (Figs. 5a and b) was not yet as clear in Virkkula et al. (2011) as it is now. For the σ_{sca} and σ_{bsca}, two local maxima occurred during late winter (February) and late summer (July). The local minima occur during spring (April) and late autumn (October). The σ_{abs} showed the highest values during winter (February) and the lowest values during summer (June). Part of this variation is explained by boundary layer dynamics. In summer, the boundary layer is higher and well mixed thus diluting the aerosol concentration. In winter the situation is the opposite and the pollution accumulates in the shallow boundary layer.

For the extensive properties, the highest values occurred at the same time in winter (February) when the ω_0 was also low, which means that there were larger amounts of particles from anthropogenic sources than in summer. Hyvärinen et al. (2011) observed increased equivalent eBC concentrations at SMEAR II in winter, when the long-range transport brings pollution from the central and eastern Europe. However, Hienola et al. (2013) estimated that about 70 % of the measured eBC at SMEAR II is emitted from local or regional sources or transported from Finnish cities so also the local and regional emissions have a significant role in the elevated eBC concentrations. Since February is one of the coldest months in Finland, domestic wood burning in the local and regional area increases the particle concentration (Karvosenoja et al., 2011). Pollution can also be transported from nearby cities (the largest and closest are Tampere and Jyväskylä). Hyvärinen et al. (2011) observed no remarkable changes in the Hyytiälä eBC concentrations coming from the Tampere region. However, the largest concentrations they observed came from the direction of Orivesi, a small town (population about 9 000) 20 km from the measurement station.

In summer, the ω_0 had its highest values since the σ_{sca} was high and the σ_{abs} was low. In summer, the anthropogenic influence is not as strong as in the winter since the energy consumption is lower. The contribution of particles from natural sources increased during spring and summer when the vegetation was active and growing. The seasonal variation in the *n* and *k* was clearly associated with the ω_0. In summer when the ω_0 was high, *n* was high and *k* was low. In winter, the relationship was the opposite. The scattering maximum in summer was probably caused by secondary organic particles (Tunved et al., 2006) explaining why the *b* and α_{sca} are also maximal.

There is an anti-correlation between the seasonal variations of ω_0 and α_{abs}. The maximum values of α_{abs} (> 1) occur in winter, which means that light is absorbed more efficiently at shorter wavelengths than in summer. A higher α_{abs} may suggest that light is absorbed not only by BC, but also by some light-absorbing organic carbon compounds, i.e. brown carbon (BrC). In using only α_{abs}, it is difficult to determine if the particles consist of BrC, since BC particles with coating can also have an α_{abs} up to 1.6 (Lack and Cappa, 2010). In Fig. 5 we can see that the value of 1.6 is not really reached at SMEAR II. Since α_{abs} is dependent on the size of the BC core, the thickness of the coating and the *m* of the coating, more detailed investigation would be needed to determine why α_{abs} is varies.

Also, the α_{abs} is typically associated with the source of the BC and it is often used to quantify whether the BC is traffic or wood burning related (!!! INVALID CITATION !!! (Sandradewi et al., 2008; Zotter et al., 2017)) so that high α_{abs} is a sign of wood burning. In the source apportionment, α_{abs} close to one indicates that the BC is sourced from traffic. Since we observed relatively higher α_{abs} in winter, the results are in line with the assumption of domestic wood burning that takes place during winter. However, in summer, α_{abs} was often < 1, which would yield an unphysical fraction (over a 100 %) of traffic related BC. Values below 1 could have been caused by large BC particles (D_p > 100 nm) that have a purely scattering coating (Lack and Cappa, 2010). It must be noted that the α_{abs} depends also on the correction algorithm. For example, if the σ_{abs} was corrected with the algorithm proposed by Arnott et al. (2005), the mean ± SD of α_{abs} would have been 1.36 ± 0.51 (see Table S2). Using the α_{abs}, which was determined by using the correction by Arnott et al. (2005), the results for the source apportionment would be different and they would show higher fraction of BC from wood burning. Further investigation of the complex nature of α_{abs} is omitted here.

The seasonal variation in α_{sca} and *b* depends on the seasonal variation in the size distribution of the particles. Both α_{sca} and *b* were maximal in summer and minimal in winter, suggesting that in summer, the particle population consisted of smaller particles than in winter. Closer investigation on the size distribution, which is presented in Fig. S6 and S7, reveals that in winter, the VMD_{tot} was experiencing it minimum due to a lack of coarse mode particles. This is in contrast with the observation or smaller α_{sca} and *b*. In fact, the seasonal variation of α_{sca} and *b* was explained by the seasonal variation of accumulation mode and VMD_{fine}, which is a good indicator for the shifting accumulation mode. In winter, the accumulation mode was shifted

towards larger sizes and the median of VMD_{fine} was about 350 nm. In summer the situation was the opposite and VMD_{fine} was about 250 nm.

3.5 Variation between the PM10 and PM1 measurements

Even though the average values between the optical properties of the PM10 and PM1 particles differed, their seasonal variation was similar for all the various properties. However, there was a seasonal variation in the relationship between the PM10 and PM1 extensive properties, as shown in Fig. 6. The seasonal variation in the PM1/PM10 ratio describes the impact of the coarse and fine particles on the σ_{sca} and σ_{abs}.

For the σ_{sca} the seasonal variation in the PM1/PM10 ratio was clear, but for the σ_{abs} there seemed to be no seasonal variation in the ratio whatsoever. The seasonal medians of the PM1/PM10 ration for the σ_{sca} varied from 0.7 to 0.8, and on average submicron particles caused about 75 % of the total scattering of the PM10 particles. This was apparently a lower fraction than in the previous analysis of SMEAR II scattering data. Virkkula et al. (2011) stated that the seasonal average contributions of submicron particles to the total σ_{sca} was in the range of 88–92 %, clearly more than in the present work. However, in that study the scattering size distribution and the contributions of the various size ranges were calculated from particle number size distributions with a Mie model and the physical diameters (D_p) were used whereas here the PM1 corresponds to particles smaller than the aerodynamic diameter D_a of 1 µm. With particle density of 1.7 g cm^{-3} this corresponds to the physical diameter $D_p = (1/1.7)^{½}$ 1 µm ≈ 0.77 µm. The contribution of particles smaller than 0.77 µm is approximately 85 % if it is estimated from Fig. 11 of Virkkula et al. (2011), still more than the ~75 % contribution of submicron scattering shown here. This may have resulted from the cutoff diameter of the PM1 impactor is not exactly sharp and also that the particles entering the impactor may have still been somewhat moist and thus larger than their dry size and were therefore removed from the sample stream. Further analysis of the difference is omitted here.

The maxima of the submicron particle scattering occurred in winter and summer. The summer peak coincided with the maxima of the PM10 α_{sca}, which already indicates that smaller particles play a major role in the size distribution. However, this correlation between the PM1/PM10 ratio and α_{sca} was not observed in winter. In Fig. 2 (and in Fig. S7), it can be seen that the VMD_{tot} always decreased in the wintertime indicating also the lack of coarse particles. However, on average, the accumulation mode is relatively large compared to the coarse mode and it is shifted towards the larger diameters. This is presented in the supplementary material (Figs. S6 and S7). The large accumulation mode caused α_{sca} to be low, even though there was relatively less scattering by the coarse particles.

For the σ_{abs}, the median of the PM1/PM10 ratio did not greatly vary seasonally. The PM1 particles absorbed about 90 % of the total PM10 particle absorption. So for the σ_{abs} there were no large difference in the σ_{abs} of the PM1 and PM10 particles. The

~~coarse mode particles are typically primary and they have a quite high ω_0 so their absorption is minor compared with the PM1 particles. The soot particles, which account for most of the particulate absorption, are typically submicron particles.~~

~~The deviation of the σ_{abs} PM1/PM10 ratio clearly varied seasonally. In summer, the variation was considerably higher than in winter. In the correction algorithm, which was used for the absorption data (Eq. 3), part of the σ_{sca} is subtracted from σ_{abs} as an apparent absorption (Muller et al., 2011). This subtraction causes relatively high uncertainty when the σ_{abs} is low and σ_{sca} is high like it is in summer. This uncertainty is emphasized for PM10 measurements, since the σ_{sca} is relatively higher than σ_{abs} if compared to PM1 measurements. The uncertainty in the measurements also explains why there were so many values above 1 measured in the PM1/PM10 σ_{abs} ratio.~~

~~The evolution of the PM1/PM10 ratios were also investigated but we observed no statistically significant trends for either σ_{sca} or σ_{abs}.~~

3.~~3~~6 Seasonality and long-term trend of ~~R~~radiative forcing efficiency

To study the climate impact of the aerosol particles, ~~For~~ the aerosol radiative forcing efficiency (RFE) the ~~mean~~ average values, trends, and seasonal variations were ~~also~~ investigated. We determined three different kind of RFE: 1) $RFE_{H\&S}$ was calculated to dry aerosol particles by using global average values suggested by Haywood and Shine (1995), 2) RFE_S was calculated also to dry aerosols but here we used more realistic environmental parameters (D, R_S, and A_C) at SMEAR II and here also the seasonality of the parameters was taken into account, and 3) $RFE_{S,moist}$ also used the more realistic and seasonally varying environmental parameters but here we took into account effect of ambient RH on ω_0 and b. The statistics of the $RFE_{H\&S}$, RFE_S and $RFE_{S,moist}$ are presented in Table 1 and their time series and seasonal variations are presented in Fig. 6~~7~~.

In general, the aerosols~~,~~ measured at SMEAR II~~,~~ tended to have a cooling effect on the climate (RFE < 0) as seen in Table 1. By using the global average values suggested by Haywood and Shine (1995), the mean $RFE_{H\&S}$ was -22 Wm^{-2}. This wa~~i~~s about 12 % less negative than the mean $RFE_{H\&S}$ (about -25 Wm^{-2}) determined by Sherman et al. (2015) for different North American stations. The difference is explained by higher mean ω_0 (about 0.91) observed by Sherman et al. (2015)~~.,~~ T~~t~~he mean b (about 0.14) was similar if compared to average values observed at SMEAR II. ~~Also, a~~A mean $RFE_{H\&S}$ -25 Wm^{-2} was determined also at SORPES station in Nanjing, China (Shen et al., 2018). Shen et al. (2018) observed a lower mean b (0.12 at 520 nm), which would increase the $RFE_{H\&S}$. However, they also observed a~~-~~ notably higher mean ω_0~~ω_0~~ (0.93 at 520 nm) at SORPES and that overcame the effect of lower ~~n~~ b.~~what we observed at SMEAR II (0.87), but for the b the situation was the opposite and it was lower at SORPES (0.12 at 525 nm) than at SMEAR II (0.14 at 550 nm). This would suggest that for dry particles the variation of ω_0 is more pronounced than the variation of b in context of calculating the $RFE_{H\&S}$.~~

~~This is also observed at SMEAR II (Fig. S9).~~ If the seasonal variation of D, A_C, and R_S were taken into account, the RFE became more negative at SMEAR II. The median~~the mean~~ RFE_S, which takes the seasonality of the environmental parameters into account, was (~~-26~~34 Wm^{-2}, ~~) was~~ lower than the median ~~more negative than~~ $RFE_{H\&S}$, which was ~~-~~23~~-~~ Wm^{-2}. This was mainly due to the higher D, and lower R_S and A_C in summer. If the ambient RH was taken into account, the median for the r (-24 Wm^{-2}) increased a bit compared to RFE_S. Taking the ambient RH (that was RH > 40 % every month) into account increases the ω_0 due to increase in the scattering. At the same time the b decreases since the particles grow in size and scatter relatively less light backwards (Birmili et al., 2009). These two changes have opposite effects on the RFE: increasing ω_0 decreases the RFE, and decreasing b increases the RFE. Here the decreasing b overcomes the effect of ω_0 and therefore the median $RFE_{S,moist}$ is higher than that of RFE_S.

~~Both,~~The long-term trends of ~~the~~ ω_0 and b tended to increase, which makes the $RFE_{H\&S}$ to decrease (i.e., become more negative). The decreasing $RFE_{H\&S}$ means that the properties of dry aerosol particles have changed so that they cool the climate more efficiently. The trends for the $RFE_{H\&S}$, RFE_S and $RFE_{S,moist}$ are presented in Table 3 as well. Since we used seasonal averages in calculating the RFE_S and $RFE_{S,moist}$, their trends we~~a~~re also depended only on the changes of the ω_0 and b and thus their trends are also decreasing and similar in magnitude as the trend for $RFE_{H\&S}$. However, in reality the trend of RFE_S and $RFE_{S,moist}$, which take into account the realistic environmental parameters, do~~es~~ not depend only on the ω_0 and b. For example, a decrease in the snow cover due to global warming would decrease the R_S and make the decrease of RFE_S and $RFE_{S,moist}$ ~~RFE~~ steeper. Here, we omitted further analysis on the effect that the changes of A_C, R_S, T_{at} and RH have on the RFE_S and $RFE_{S,moist}$.

The seasonal variation in the $RFE_{H\&S}$ followed the seasonal cycles of the ω_0 and b. The $RFE_{H\&S}$ was minimal in summer and maximal in winter. Since b was lowest (forward-scattering particles) and the ω_0 is also low (dark particles) in winter, the particles clearly did not have as strong a cooling effect as in summer when particles are smaller and light colored. If the seasonal changes of D, A_C, and R_S, were taken into account, the seasonal variability of RFE_S ~~is~~ amplified remarkably ~~compared to $RFE_{H\&S}$~~ as seen in Fig. 7b. In winter, the higher R_S causes the aerosol particles to be less cooling or even warming, but ~~In winter,~~since the D is low~~er~~ and the A_C ~~is~~ high~~er,~~ (see~~which are shown in~~ Fig. S1), ~~causing~~ the aerosol particles to have less effect (RFE closer to zero) than in summer. ~~During winter the higher R_S causes the aerosol particles to be less cooling or even warming.~~ We chose to use the R_S determined for a boreal forest according to the surroundings of SMEAR II. However, the area around the station consists also of fields and lakes, which in winter~~,~~ would act as smooth snow fields. Even for snow containing impurities the R_S is notably higher (> 0.7) than R_s for snow covered boreal forest (Warren and Wiscombe, 1980). Using R_S = 0.7 for winter time data, would increase the RFE_S and amplify its seasonal variation even more.~~.~~

Taking the effect of ambient RH into account decreases the seasonality in RFE_S a bit.~~increases the ω_0 since the aerosols scatter more light due to hygroscopic growth. However, the same effect decreases the b since the particles grow in size and scatter relatively less light backwards .~~ The seasonality of RH is presented in Fig. S1d and on average the RH is higher in winter than

in summer. Fig. 7b shows that that compared to RFE_S, the $RFE_{S,moist}$ is less negative in summer ~~compared to RFE_S since~~ when the effect of RH on b overcomes the effect on ω_0. Also Fierz-Schmidhauser et al. (2010) ~~also~~ observed this kind of behavior at the Jungfraujoch station. In winter, the situation wa~~i~~s actually the opposite and the $RFE_{S,moist}$ wa~~i~~s more negative than RFE_S. However~~.~~ ~~However, in winter,~~ the ~~effect~~difference ~~of RH~~ wa~~i~~s small, partly due to the ~~small~~ low D and ~~large~~high A_C. In general, the ~~observed~~ effect of the RH on the seasonal variation of -RFE ~~i~~was smaller than the effect of taking the seasonal variation of D, A_C, and R_S into account.

The RFE (or $\Delta F \delta^{-1}$) describes only the efficiency of the aerosol particles in cooling or warming the climate per unit of aerosol optical depth (δ).

Even if the RFE was very negative, the influence of aerosol particles on the climate would be small if the δ was small. ~~The δ is highly dependent on the σ_{sca} and σ_{abs}; the more there are scattering and absorbing material in the atmosphere, the higher the δ.~~

Eq. 13 assumes that the properties of ~~the~~ aerosol particles are uniform in the atmospheric column that is rarely the case in reality. In ambient air, we should also take into account the variability in RH as a function of height, since~~. At~~ at the top of the boundary layer we typically have RH values close to 100 %. Here, we determined the RFE by using the RH measured near the ground (16 m). The simplified RFE does not give an absolute value for the aerosol forcing; however, it can still indicate how the changes in AOPs affect the climate.

~~Even if the RFE was very negative, the influence of aerosol particles on the climate would be small if the δ was small. The δ is highly dependent on the σ_{sca} and σ_{abs}; the more there are scattering and absorbing material in the atmosphere, the higher the δ.~~

3.4 Effect of excluding the moist data

Only about 62 % of AOP data measured before 2010, was marked as valid. A big fraction of the not-valid data was invalidated due to too high RH. If we took the moist data into account and estimated it to dry conditions, the data coverage from June 2006 to December 2010 increases to 87 %. To test, if excluding large amount of data had a significant difference to the results, we used Eqs. 1 and 2 to estimate the moist (RH > 40 %) σ_{sca} and σ_{bsca} to dry conditions and included this data in calculating the median values and in the trend analysis. Also, moist (RH > 40 %) σ_{abs} measurements were included here.

If the moist periods of σ_{sca} and σ_{abs} measurements were included in the analysis and the moist scattering data were estimated to dry conditions by using the parametrization suggested by Andrews et al. (2006), we would get median values of σ_{sca} = 10.4 Mm^{-1}, σ_{bsca} = 1.5 Mm^{-1}, σ_{abs} = 1.5 Mm^{-1}, ω_0 = 0.88, b = 0.14, α_{abs} = 0.97, and $RFE_{H\&S}$ = -23 Wm^{-2} for PM10 (σ_{sca}, σ_{bsca}, ω_0, b, and $RFE_{H\&S}$ at 550 nm, σ_{abs} at 520 nm, α_{abs} at 370 nm/950). Taking the moist samples into account, the σ_{sca} and σ_{abs} increase in summer and autumn (see Fig. S8). We could not determine the α_{sca}, since we only converted the σ_{sca} at 550 nm to dry

conditions. If we used the parameters observed by Zieger et al. (2015), the median σ_{sca} = 10.3 Mm^{-1}, which is very close to the value obtained by using the parameters suggested by Andrews et al. (2006). For the extensive properties, including also the moist data increased their median values about 7 % and for the intensive properties there were no notable effect. Omitting the moist data periods from the data set does not seem have a large effect on the median AOPs in this data set.

Including the originally omitted data in the trend analysis, we observed statistically significant (p-value < 0.05) trends for the PM10 σ_{sca}, σ_{bsca}, σ_{abs}, ω_0, and RFE with the slopes of -4 %yr^{-1}, -5 %yr^{-1}, -5 %yr^{-1}, 0.2 %yr^{-1}, and 0.6 %yr^{-1}, respectively. Still, there were decreasing trends for extensive properties and positive trends for ω_0. For b, there was no significant trend anymore due to. The difference between the σ_{sca} and σ_{abs} trends decreased from 3 %yr^{-1} to 1 %yr^{-1} if compared against the trends that were determined only for the dry conditions. Including the moist data and acquiring longer data sets in the trend analysis suggests that the relative difference between the trends of σ_{sca} and σ_{abs} might not be that large. ~~This is analyzed in further detail in Fig. 8, where the ω_0 is presented as a function of b. In Fig. 8 the $RFE_{H\&S}$ is presented with isolines and the σ_{sca} is presented by color coding. Fig. 8 shows that when the $RFE_{H\&S}$ is most negative, the median σ_{sca} is actually experiencing its lowest value. When the $RFE_{H\&S}$ is closest to zero, the median σ_{sca} is the highest. It is also seen that when the b is high and the particle size distribution consists of smaller particles, the particles are most efficient at cooling the atmosphere even though the average ω_0 is the lowest.~~

~~These relationships were also observed in a study of AOPs at the Station for Observing Regional Processes of the Earth System (SORPES), a measurement station in Nanjing China . Also, and observed similar systematic variability between σ_{sca}, ω_0, b, and $RFE_{H\&S}$ at several North American measurement stations; when the σ_{sca} increases, the ω_0 increases and the b decreases. Sherman et al. (2015) suggested that this variability could be caused by deposition of larger particles, which typically absorb less light. observed that $RFE_{H\&S}$ increases (i.e. becomes less negative) with increasing σ_{sca}, but Sherman et al. (2015) did not observe this trend.~~

4 Summary and conclusions

In this study, we presented ~~over~~ 11.5-year ~~-~~long time series of AOPs measured at SMEAR II, a ~~a~~ station in southern Finland. ~~With the long time series, it was possible to see statistically significant trends, seasonal variation, and different types of causalities between the optical properties. We compared the AOPs with the aerosol size distribution measurements conducted at the station and observed in detail how the AOPs are dependent on the shape of the size distribution. By comparing the AOPs and size distribution, we were able to determine the m values that can be used in modeling the σ_{sca} and σ_{abs} from size distribution measurements~~Compared to regional and rural European ~~,~~sites, the σ_{sca} at the boreal SMEAR II station was low. However, the average σ_{sca} and σ_{abs} were higher than those observed at other Finnish measurement stations that were the arctic station in Pallas

and the semi-urban station in Kuopio, Eastern Finland. Because of the more southern location, the SMEAR II was probably more affected by regional emissions and long-transport pollution from Europe than the other Finnish measurement sites, which would explain the higher concentrations.

~~There were clear seasonal variations in the AOPs.~~ The highest σ_{sca} and σ_{abs} were measured in winter when the boundary layer is lower and the pollution is not diluted as efficiently as in summer. Transported pollution from the regional area and from Europe, also increases the concentrations in winter, when the energy consumption is higher. In winter, the ω_0 was low (i.e. absorption was relatively high compared to scattering), which also indicates that there was a higher fraction of particles from anthropogenic combustion sources. The σ_{sca} had high values also in summer but the σ_{abs} had its minimum and therefore the ω_0 reached it maximum in summer. This observation indicates that the particle concentration was high in summer due to active vegetation.

Closer investigation on the size distribution revealed that ~~The largest differences occur during summer and winter. The seasonal variations in the extensive properties, ω_0 and size distribution revealed that in winter the particles have a larger contribution from the anthropogenic sources than during summer.~~ the seasonal variations of b and α_{sca} were caused by shifting accumulation mode and not by concentration of coarse mode particles. In summer, b and α_{sca} had their maxima (i.e. there was a higher fraction of smaller accumulation mode particles); and in winter, they had their minima (i.e. there was a higher fraction of large accumulation mode particles).

The extensive AOPs, as well as the aerosol number and volume concentration, tended to decrease. Our observations w~~as~~ere in line with the other studies conducted in Europe and North America, which ~~that~~ also observed decreasing trends for the extensive AOPs (Collaud Coen et al., 2013; Pandolfi et al., 2018; Sherman et al., 2015), number concentration (Asmi et al., 2013) and aerosol optical depth (Li et al., 2014). This uniform decreasing trend in the amount of aerosol particles suggests that the anthropogenic emissions ~~of particulate matter and gases that take part in secondary aerosol formation~~ ha~~s~~ve been decreasing in Europe and North America. The observed tendency for b and α_{sca} to increase together with the decreasing extensive properties indicated that the particle size distribution consisted of less larger particles. A more detailed investigation revealed that the number of larger accumulation mode particles (500–800 nm in diameter) decreased relatively the fastest, which ~~also supports the assumed~~would indicate a decrease in transported anthropogenic pollution~~.~~

~~There were clear seasonal variations in the AOPs. The largest differences occur during summer and winter. The seasonal variations in the extensive properties, ω_0 and size distribution revealed that in winter the particles have a larger contribution from the anthropogenic sources than duri~~ at SMEAR II.~~ng summer.~~

Since the aerosol particles were scattering light more efficiently to backward hemisphere~~are smaller~~ and because they were less dark than before, their RFE tended to decrease (i.e. became more negative), which means that the ability of aerosols to cool the climate per unit δ increased. However, since the extensive properties and particle number concentration ~~are~~ were decreasing, which means that the δ ~~decreases~~ decreased as well, the total aerosol forcing ~~is~~ was probably also decreasing. ~~We determined the RFE to dry aerosol particles by using global average values suggested by . To test the sensitivity of RFE to environmental parameters (D, R_S, and A_C), we calculated the RFE also by using more realistic and seasonally averaged environmental parameters. We also determined the RFE for ambient RH, since it is affected by the hygroscopic growth of aerosols. We observed that at SMEAR II the environmental parameters had a higher impact on the RFE than the ambient RH.~~ Here, we only studied the effect of AOPs on the RFE. ~~T~~Studying and taking also the long-term trends of the environmental parameters into account would give more realistic~~probably have a large effect on the~~ trend for~~of~~ the RFE.

Data availability All the data presented in this study is open access. The optical properties and the size distribution data from SMEAR II has been uploaded on the EBAS database (EBAS: http://ebas.nilu.no/, last access: 18 March 2019) run by the Norwegian Institute for Air Research (NILU). Meteorological parameters measured at SMEAR II, such as the RH used here, can be accessed by the Smart-SMEAR online tool (Junninen et al., 2009). Also the Finnish Meteorological Institute provides open access data and we used their online data tool (FMI: https://ilmatieteenlaitos.fi/havaintojen-lataus, last access: 18 March 2019) to access the ceilometer data measured at Halli airport.

Author contribution Krista Luoma did the data analysis and wrote the manuscript together with Aki Virkkula. Pasi Aalto and Aki Virkkula have set up the long term measurements of AOPs at SMEAR II. All authors reviewed and commented on the manuscript.

Acknowledgements The research leading to these results has received funding from the European Union Seventh Framework Programme under grant agreement No 262254. This research has also received funding from the European Union's Horizon 2020 research and innovation programme under grant agreement No 654109 via project ACTRIS-2 and grant agreement No 689443 via project iCUPE. The work was also funded by the Academy of Finland (project. No 307331).

References

Aalto, P., Hämeri, K., Becker, E., Weber, R., Salm, J., Mäkelä, J. M., Hoell, C., O'dowd, C. D., Hansson, H.-C., and Väkevä, M.: Physical characterization of aerosol particles during nucleation events, Tellus B: Chemical and Physical Meteorology, 53, 344-358, 2001.

Anderson, T. L., and Ogren, J. A.: Determining aerosol radiative properties using the TSI 3563 integrating nephelometer, Aerosol Science and Technology, 29, 57-69, 1998.

Andrews, E., Sheridan, P., Fiebig, M., McComiskey, A., Ogren, J., Arnott, P., Covert, D., Elleman, R., Gasparini, R., and Collins, D.: Comparison of methods for deriving aerosol asymmetry parameter, Journal of Geophysical Research: Atmospheres, 111, 2006.

Andrews, E., Ogren, J., Bonasoni, P., Marinoni, A., Cuevas, E., Rodríguez, S., Sun, J. Y., Jaffe, D., Fischer, E., and Baltensperger, U.: Climatology of aerosol radiative properties in the free troposphere, Atmospheric Research, 102, 365-393, 2011.

Andrews, E., Sheridan, P. J., Ogren, J. A., Hageman, D., Jefferson, A., Wendell, J., Alástuey, A., Alados-Arboledas, L., Bergin, M., and Ealo, M.: Overview of the NOAA/ESRL federated aerosol network, Bulletin of the American Meteorological Society, 100, 123-135, 2019.

Arnott, W. P., Hamasha, K., Moosmüller, H., Sheridan, P. J., and Ogren, J. A.: Towards aerosol light-absorption measurements with a 7-wavelength aethalometer: Evaluation with a photoacoustic instrument and 3-wavelength nephelometer, Aerosol Science and Technology, 39, 17-29, 2005.

Asmi, A., Collaud Coen, M., Ogren, J., Andrews, E., Sheridan, P., Jefferson, A., Weingartner, E., Baltensperger, U., Bukowiecki, N., and Lihavainen, H.: Aerosol decadal trends–Part 2: In-situ aerosol particle number concentrations at GAW and ACTRIS stations, Atmospheric Chemistry and Physics, 13, 895-916, 2013.

Backman, J., Schmeisser, L., Virkkula, A., Ogren, J. A., Asmi, E., Starkweather, S., Sharma, S., Eleftheriadis, K., Uttal, T., and Jefferson, A.: On Aethalometer measurement uncertainties and an instrument correction factor for the Arctic, Atmospheric Measurement Techniques, 2017.

Bergin, M. H., Ogren, J. A., Schwartz, S. E., and McInnes, L. M.: Evaporation of ammonium nitrate aerosol in a heated nephelometer: Implications for field measurements, Environmental Science & Technology, 31, 2878-2883, 1997.

Birmili, W., Schwirn, K., Nowak, A., Petäjä, T., Joutsensaari, J., Rose, D., Wiedensohler, A., Hämeri, K., Aalto, P., and Kulmala, M.: Measurements of humidified particle number size distributions in a Finnish boreal forest: derivation of hygroscopic particle growth factors, Boreal Environment Research, 14, 458-480, 2009.

Carrico, C. M., Kus, P., Rood, M. J., Quinn, P. K., and Bates, T. S.: Mixtures of pollution, dust, sea salt, and volcanic aerosol during ACE-Asia: Radiative properties as a function of relative humidity, Journal of Geophysical Research: Atmospheres, 108, 2003.

Charlson, R. J., Schwartz, S., Hales, J., Cess, R. D., Coakley, J. J., Hansen, J., and Hofmann, D.: Climate forcing by anthropogenic aerosols, Science, 255, 423-430, 1992.

Collaud Coen, M., Weingartner, E., Nyeki, S., Cozic, J., Henning, S., Verheggen, B., Gehrig, R., and Baltensperger, U.: Long-term trend analysis of aerosol variables at the high-alpine site Jungfraujoch, Journal of Geophysical Research: Atmospheres, 112, 2007.

Collaud Coen, M., Weingartner, E., Apituley, A., Ceburnis, D., Fierz-Schmidhauser, R., Flentje, H., Henzing, J., Jennings, S. G., Moerman, M., and Petzold, A.: Minimizing light absorption measurement artifacts of the Aethalometer: evaluation of five correction algorithms, Atmospheric Measurement Techniques, 3, 457-474, 2010.

Collaud Coen, M., Andrews, E., Asmi, A., Baltensperger, U., Bukowiecki, N., Day, D., Fiebig, M., Fjæraa, A. M., Flentje, H., and Hyvärinen, A.: Aerosol decadal trends–Part 1: In-situ optical measurements at GAW and IMPROVE stations, Atmospheric Chemistry and Physics, 13, 869-894, 2013.

Delene, D. J., and Ogren, J. A.: Variability of aerosol optical properties at four North American surface monitoring sites, Journal of the Atmospheric Sciences, 59, 1135-1150, 2002.

Ehn, M., Thornton, J. A., Kleist, E., Sipilä, M., Junninen, H., Pullinen, I., Springer, M., Rubach, F., Tillmann, R., and Lee, B.: A large source of low-volatility secondary organic aerosol, Nature, 506, 476, 2014.

Fierz-Schmidhauser, R., Zieger, P., Gysel, M., Kammermann, L., DeCarlo, P., Baltensperger, U., and Weingartner, E.: Measured and predicted aerosol light scattering enhancement factors at the high alpine site Jungfraujoch, Atmospheric Chemistry and Physics, 10, 2319-2333, 2010.

Gilbert, R. O.: Statistical methods for environmental pollution monitoring, John Wiley & Sons, 1987.

Gyawali, M., Arnott, W., Lewis, K., and Moosmüller, H.: In situ aerosol optics in Reno, NV, USA during and after the summer 2008 California wildfires and the influence of absorbing and non-absorbing organic coatings on spectral light absorption, Atmospheric Chemistry and Physics, 9, 8007-8015, 2009.

Hari, P., and Kulmala, M.: Station for Measuring Ecosystem–Atmosphere Relations, Boreal Environment Research, 10, 315-322, 2005.

Hari, P., Nikinmaa, E., Pohja, T., Siivola, E., Bäck, J., Vesala, T., and Kulmala, M.: Station for measuring ecosystem-atmosphere relations: SMEAR, in: Physical and Physiological Forest Ecology, Springer, 471-487, 2013.

Haywood, J., and Shine, K.: The effect of anthropogenic sulfate and soot aerosol on the clear sky planetary radiation budget, Geophysical Research Letters, 22, 603-606, 1995.

Hienola, A., Pietikäinen, J.-P., Jacob, D., Pozdun, R., Petäjä, T., Hyvärinen, A.-P., Sogacheva, L., Kerminen, V.-M., Kulmala, M., and Laaksonen, A.: Black carbon concentration and deposition estimations in Finland by the regional aerosol-climate model REMO-HAM, Atmospheric Chemistry and Physics, 13, 4033, 2013.

Hyvärinen, A.-P., Kolmonen, P., Kerminen, V.-M., Virkkula, A., Leskinen, A., Komppula, M., Hatakka, J., Burkhart, J., Stohl, A., and Aalto, P.: Aerosol black carbon at five background measurement sites over Finland, a gateway to the Arctic, Atmospheric Environment, 45, 4042-4050, 2011.

Junninen, H., Lauri, A., Keronen, P., Aalto, P., Hiltunen, V., Hari, P., and Kulmala, M.: Smart-SMEAR: on-line data exploration and visualization tool for SMEAR stations, Boreal Environment Research, 14, 447-457, 2009.

Karvosenoja, N., Kangas, L., Kupiainen, K., Kukkonen, J., Karppinen, A., Sofiev, M., Tainio, M., Paunu, V.-V., Ahtoniemi, P., and Tuomisto, J. T.: Integrated modeling assessments of the population exposure in Finland to primary PM2. 5 from traffic and domestic wood combustion on the resolutions of 1 and 10 km, Air Quality, Atmosphere & Health, 4, 179-188, 2011.

Kulmala, M., Vehkamäki, H., Petäjä, T., Dal Maso, M., Lauri, A., Kerminen, V.-M., Birmili, W., and McMurry, P.: Formation and growth rates of ultrafine atmospheric particles: a review of observations, Journal of Aerosol Science, 35, 143-176, 2004.

Kulmala, M., Kontkanen, J., Junninen, H., Lehtipalo, K., Manninen, H. E., Nieminen, T., Petäjä, T., Sipilä, M., Schobesberger, S., and Rantala, P.: Direct observations of atmospheric aerosol nucleation, Science, 339, 943-946, 2013.

Kuusinen, N., Kolari, P., Levula, J., Porcar-Castell, A., Stenberg, P., and Berninger, F.: Seasonal variation in boreal pine forest albedo and effects of canopy snow on forest reflectance, Agricultural and Forest Meteorology, 164, 53-60, 2012.

Lack, D., and Cappa, C.: Impact of brown and clear carbon on light absorption enhancement, single scatter albedo and absorption wavelength dependence of black carbon, Atmospheric Chemistry and Physics, 10, 4207-4220, 2010.

Laj, P., Klausen, J., Bilde, M., Plass-Duelmer, C., Pappalardo, G., Clerbaux, C., Baltensperger, U., Hjorth, J., Simpson, D., and Reimann, S.: Measuring atmospheric composition change, Atmospheric Environment, 43, 5351-5414, 2009.

Leskinen, A., Arola, A., Komppula, M., Portin, H., Tiitta, P., Miettinen, P., Romakkaniemi, S., Laaksonen, A., and Lehtinen, K.: Seasonal cycle and source analyses of aerosol optical properties in a semi-urban environment at Puijo station in Eastern Finland, Atmospheric Chemistry and Physics, 12, 5647, 2012.

Li, J., Carlson, B. E., Dubovik, O., and Lacis, A. A.: Recent trends in aerosol optical properties derived from AERONET measurements, Atmospheric Chemistry and Physics, 14, 12271-12289, 2014.

Lihavainen, H., Hyvärinen, A., Asmi, E., Hatakka, J., and Viisanen, Y.: Long-term variability of aerosol optical properties in northern Finland, Boreal Environment Research, 20, 526-541, 2015.

Lohmann, U., and Feichter, J.: Global indirect aerosol effects: a review, Atmospheric Chemistry and Physics, 5, 715-737, 2005.

Muller, T., Henzing, J., De Leeuw, G., Wiedensohler, A., Alastuey, A., Angelov, H., Bizjak, M., Coen, M., Engstrom, J., and Gruening, C.: Characterization and intercomparison of aerosol absorption photometers: result of two intercomparison workshops, Atmospheric Measurement Techniques, 4, 245-268, 2011.

Mätzler, C.: MATLAB functions for Mie scattering and absorption, version 2, Institut für Angewandte Physik, University of Bern, 2002.

Nessler, R., Weingartner, E., and Baltensperger, U.: Effect of humidity on aerosol light absorption and its implications for extinction and the single scattering albedo illustrated for a site in the lower free troposphere, Journal of Aerosol Science, 36, 958-972, 2005.

Ogren, J. A.: A systematic approach to in situ observations of aerosol properties, Aerosol forcing of climate, 215-226, 1995.

Pandolfi, M., Alados-Arboledas, L., Alastuey, A., Andrade, M., Angelov, C., Artiñano, B., Backman, J., Baltensperger, U., Bonasoni, P., and Bukowiecki, N.: A European aerosol phenomenology–6: scattering properties of atmospheric aerosol particles from 28 ACTRIS sites, Atmospheric Chemistry and Physics, 18, 7877-7911, 2018.

Ramanathan, V., Crutzen, P., Kiehl, J., and Rosenfeld, D.: Aerosols, climate, and the hydrological cycle, Science, 294, 2119-2124, 2001.

Sandradewi, J., Prévôt, A. S., Szidat, S., Perron, N., Alfarra, M. R., Lanz, V. A., Weingartner, E., and Baltensperger, U.: Using aerosol light absorption measurements for the quantitative determination of wood burning and traffic emission contributions to particulate matter, Environmental Science & Technology, 42, 3316-3323, 2008.

Schnaiter, M., Linke, C., Möhler, O., Naumann, K. H., Saathoff, H., Wagner, R., Schurath, U., and Wehner, B.: Absorption amplification of black carbon internally mixed with secondary organic aerosol, Journal of Geophysical Research: Atmospheres, 110, 2005.

Schuster, G. L., Dubovik, O., and Holben, B. N.: Angstrom exponent and bimodal aerosol size distributions, Journal of Geophysical Research: Atmospheres, 111, 2006.

Shen, Y., Virkkula, A., Ding, A., Wang, J., Chi, X., Nie, W., Qi, X., Huang, X., Liu, Q., and Zheng, L.: Aerosol optical properties at SORPES in Nanjing, east China, Atmospheric Chemistry and Physics, 18, 5265-5292, 2018.

Sheridan, P. J., and Ogren, J. A.: Observations of the vertical and regional variability of aerosol optical properties over central and eastern North America, Journal of Geophysical Research: Atmospheres, 104, 16793-16805, 1999.

Sherman, J., Sheridan, P., Ogren, J., Andrews, E., Hageman, D., Schmeisser, L., Jefferson, A., and Sharma, S.: A multi-year study of lower tropospheric aerosol variability and systematic relationships from four North American regions, Atmospheric Chemistry and Physics, 15, 12487-12517, 2015.

Stocker, T. F. a. Q., Dahe and Plattner, Gian-Kasper and Tignor, Melinda and Allen, Simon K and Boschung, Judith and Nauels, Alexander and Xia, Yu and Bex, Vincent and Midgley, Pauline M: Climate change 2013: The physical science basis, 2013.

Tunved, P., Hansson, H.-C., Kerminen, V.-M., Ström, J., Dal Maso, M., Lihavainen, H., Viisanen, Y., Aalto, P., Komppula, M., and Kulmala, M.: High natural aerosol loading over boreal forests, Science, 312, 261-263, 2006.

Tørseth, K., Aas, W., Breivik, K., Fjæraa, A. M., Fiebig, M., Hjellbrekke, A.-G., Lund Myhre, C., Solberg, S., and Yttri, K. E. J. A. C.: Introduction to the European Monitoring and Evaluation Programme (EMEP) and observed atmospheric composition change during 1972–2009, Atmospheric Chemistry and Physics, 12, 5447-5481, 2012.

Warren, S. G., and Wiscombe, W. J. J. J. o. t. A. S.: A model for the spectral albedo of snow. II: Snow containing atmospheric aerosols, 37, 2734-2745, 1980.

Weatherhead, E. C., Wielicki, B. A., Ramaswamy, V., Abbott, M., Ackerman, T. P., Atlas, R., Brasseur, G., Bruhwiler, L., Busalacchi, A. J., and Butler, J. H.: Designing the climate observing system of the future, Earth's Future, 6, 80-102, 2018.

Wild, M.: Global dimming and brightening: A review, Journal of Geophysical Research: Atmospheres, 114, 2009.

Wild, M.: Enlightening global dimming and brightening, Bulletin of the American Meteorological Society, 93, 27-37, 2012.

Virkkula, A., Backman, J., Aalto, P., Hulkkonen, M., Riuttanen, L., Nieminen, T., Dal Maso, M., Sogacheva, L., De Leeuw, G., and Kulmala, M.: Seasonal cycle, size dependencies, and source analyses of aerosol optical properties at the SMEAR II measurement station in Hyytiala, Finland, Atmospheric Chemistry and Physics, 11, 4445, 2011.

WMO/GAW: Aerosol Measurement Procedures, Guidelines and Recommendations, GAW Report No. 153, World Meteorological Organization, Geneva, Switzerland, 2003.

WMO/GAW: Recommendations for a Composite Surface-Based Aerosol Network, GAW Report No. 207, World Meteorological Organization, Geneva, Switzerland, 2012.

WMO/GAW: Aerosol Measurement Procedures, Guidelines and Recommendations, 2nd edition, GAW Report No. 227, World Meteorological Organization, Geneva, Switzerland, 2016.

Zhang, R., Khalizov, A. F., Pagels, J., Zhang, D., Xue, H., and McMurry, P. H.: Variability in morphology, hygroscopicity, and optical properties of soot aerosols during atmospheric processing, Proceedings of the National Academy of Sciences, 105, 10291-10296, 2008.

Zieger, P., Aalto, P., Aaltonen, V., Äijälä, M., Backman, J., Hong, J., Komppula, M., Krejci, R., Laborde, M., and Lampilahti, J.: Low hygroscopic scattering enhancement of boreal aerosol and the implications for a columnar optical closure study, Atmospheric Chemistry and Physics, 15, 7247-7267, 2015.

Zotter, P., Herich, H., Gysel, M., El-Haddad, I., Zhang, Y., Močnik, G., Hüglin, C., Baltensperger, U., Szidat, S., and Prévôt, A. S.: Evaluation of the absorption Ångström exponents for traffic and wood burning in the Aethalometer-based source apportionment using radiocarbon measurements of ambient aerosol, Atmospheric Chemistry and Physics, 17, 4229-4249, 2017.

Ångström, A.: On the atmospheric transmission of sun radiation and on dust in the air, Geografiska Annaler, 11, 156-166, 1929.

Table 11: ~~Average~~ Descriptive statistics~~values~~ of the AOPs for the PM10 particles. The average values were calculated from all valid data.

PM10	λ (nm)	mean ± SD	1 %	10 %	25 %	50 %	75 %	90 %	99 %
σ_{sca} (Mm^{-1})	450	21.8 ± 23.3	1.8	4.5	7.6	14.2	26.8	48.5	114.1
	550	15.2 ± 16.7	1.3	3.4	5.5	9.8	18.3	33.4	82.5
	700	9.5 ± 10.5	0.8	2.3	3.7	6.3	11.3	20.3	52.3
σ_{bsca} (Mm^{-1})	450	2.5 ± 2.9	0.2	0.6	1.0	1.8	3.2	5.3	11.1
	550	2.0 ± 1.8	0.2	0.5	0.8	1.4	2.5	4.2	8.8
	700	1.6 ± 1.5	0.2	0.4	0.7	1.2	2.0	3.4	7.4
σ_{abs} (Mm^{-1})	370	3.0 ± 3.6	0.2	0.6	1.0	1.9	3.6	6.6	18.1
	470	2.5 ± 2.9	0.2	0.5	0.8	1.6	3.0	5.4	14.3
	520	2.2 ± 2.4	0.1	0.4	0.7	1.4	2.6	4.7	12.3
	590	1.9 ± 2.2	0.1	0.4	0.7	1.3	2.4	4.2	10.8
	660	1.8 ± 2.0	0.1	0.3	0.6	1.2	2.2	3.8	9.9
	880	1.3 ± 1.4	0.1	0.3	0.5	0.9	1.6	2.9	7.2
	950	1.2 ± 1.3	0.1	0.3	0.4	0.8	1.5	2.6	6.5
ω_0	450	0.88 ± 0.07	0.64	0.80	0.85	0.89	0.93	0.95	0.98
	550	0.87 ± 0.07	0.62	0.78	0.84	0.88	0.92	0.94	0.98
	700	0.84 ± 0.08	0.55	0.74	0.80	0.85	0.90	0.93	0.97
b	450	0.13 ± 0.03	0.08	0.10	0.11	0.12	0.14	0.16	0.21
	550	0.14 ± 0.03	0.09	0.11	0.13	0.14	0.16	0.17	0.21
	700	0.19 ± 0.07	0.07	0.13	0.15	0.18	0.21	0.25	0.44
α_{sca}	450/550	1.73 ± 0.52	0.23	1.03	1.49	1.82	2.09	2.29	2.58
	450/700	1.80 ± 0.55	0.32	1.00	1.53	1.88	2.17	2.39	2.80
	550/700	1.85 ± 0.64	0.23	0.95	1.53	1.95	2.26	2.50	3.15
α_{abs}	370/520	0.95 ± 0. 48	-0.29	0.51	0.76	0.98	1.16	1.32	1.97
	370/950	0.95 ± 0.36	-0.16	0.55	0.80	0.99	1.13	1.24	1.69
	470/660	0.95 ± 0.49	-0.52	0.52	0.80	1.01	1.15	1.29	2.07
	470/950	0.99 ± 0.41	-0.32	0.58	0.86	1.06	1.18	1.28	1.83
	660/950	1.02 ± 0.57	-0.77	0.57	0.90	1.11	1.23	1.34	2.17
n	450	1.541 ± 0.065	1.330	1.478	1.512	1.542	1.572	1.607	1.697
	550	1.518 ± 0.067	1.289	1.452	1.490	1.522	1.550	1.581	1.674
	700	1.491 ± 0.091	1.247	1.379	1.454	1.501	1.536	1.574	1.740
k	450	0.021 ± 0.020	0.002	0.006	0.009	0.016	0.026	0.039	0.097
	550	0.020 ± 0.018	0.002	0.006	0.010	0.016	0.025	0.038	0.089
	700	0.022 ± 0.019	0.003	0.007	0.011	0.018	0.027	0.041	0.092
$RFE_{H\&S}$ (Wm^{-2})	550	-22 ± 6	-32	-28	-26	-23	-19	-16	-3
RFE_{S} (Wm^{-2})	550	-35 ± 32	-97	-82	-67	-26	-5	0	12
$RFE_{S,moist}$ (Wm^{-2})	550	~~-32~~ 33 ± 28	~~-85~~88	~~-72~~74	~~-60~~62	-24	-5	-2	~~5~~4

Table 22: ~~Average values~~Descriptive statistics of the AOPs for the PM1 particles. The average values were calculated from all valid data; therefore if compared with the PM10 average values, there is a 4-year shorter dataset.

PM1	λ (nm)	mean ± SD	1 %	10 %	25 %	50 %	75 %	90 %	99 %
σ_{sca} (Mm^{-1})	450	17.7 ± 19.2	1.2	3.1	5.6	11.3	22.3	40.4	96.1
	550	11.4 ± 13.0	0.8	2.1	3.6	7.1	14.1	26.1	64.8
	700	6.3 ± 7.5	0.4	1.2	2.0	3.8	7.6	14.4	37.4
σ_{bsca} (Mm^{-1})	450	2.1 ± 2.0	0.2	0.4	0.8	1.4	2.7	4.5	9.7
	550	1.6 ± 1.5	0.1	0.3	0.6	1.1	2.0	3.4	7.5
	700	1.2 ± 1.2	0.1	0.3	0.5	0.8	1.5	2.6	5.9
σ_{abs} (Mm^{-1})	370	2.4 ± 2.9	0.1	0.4	0.8	1.6	2.9	5.2	15.0
	470	2.0 ± 2.3	0.1	0.4	0.7	1.3	2.4	4.3	11.7
	520	1.7 ± 1.9	0.1	0.3	0.6	1.2	2.1	3.7	10.0
	590	1.6 ± 1.7	0.1	0.3	0.5	1.0	1.9	3.3	8.8
	660	1.4 ± 1.6	0.1	0.3	0.5	01.0	1.8	3.1	8.0
	880	1.1 ± 1.1	0.1	0.2	0.4	0.7	1.3	2.3	5.8
	950	0.9 ± 1.0	0.0	0.2	0.3	0.6	1.2	2.0	5.1
ω_0	450	0.88 ± 0.08	0.62	0.78	0.84	0.89	0.93	0.96	0.98
	550	0.85 ± 0.08	0.59	0.75	0.81	0.87	0.91	0.94	0.98
	700	0.80 ± 0.10	0.48	0.67	0.75	0.81	0.87	0.91	0.96
b	450	0.13 ± 0.03	0.07	0.10	0.11	0.13	0.14	0.17	0.23
	550	0.15 ± 0.03	0.09	0.12	0.13	0.15	0.17	0.19	0.24
	700	0.23 ± 0.13	-0.06	0.14	0.17	0.21	0.26	0.34	0.78
α_{sca}	450/700	2.22 ± 0.44	0.88	1.70	1.99	2.28	2.51	2.66	2.95
	450/550	2.36 ± 0.55	0.74	1.76	2.09	2.41	2.66	2.87	3.70
	550/700	2.48 ± 0.81	0.25	1.73	2.16	2.52	2.82	3.13	4.69
α_{abs}	370/520	0.96 ± 0.61	-0.67	0.47	0.74	0.99	1.20	1.39	2.32
	370/950	0.97 ± 0.44	-0.36	0.52	0.80	1.03	1.19	1.33	1.96
	470/660	0.94 ± 0.66	-0.94	0.46	0.76	1.00	1.17	1.33	2.35
	470/950	1.03 ± 0.51	-0.51	0.56	0.87	1.11	1.25	1.39	2.24
	660/950	1.13 ± 0.72	-1.10	0.60	0.97	1.20	1.35	1.54	2.96
n	450	1.509 ± 0.057	1.348	1.441	1.478	1.513	1.542	1.568	1.634
	550	1.484 ± 0.054	1.338	1.422	1.456	1.487	1.516	1.540	1.598
	700	1.471 ± 0.074	1.294	1.393	1.435	1.472	1.505	1.537	1.677
k	450	0.025 ± 0.020	0.003	0.008	0.013	0.020	0.031	0.045	0.099
	550	0.025 ± 0.018	0.004	0.009	0.014	0.021	0.031	0.044	0.093
	700	0.028 ± 0.019	0.005	0.011	0.017	0.024	0.035	0.049	0.098

Table 33: Slopes of the trends (in absolute values and in estimated percentages per year) and their statistical significance. The lower and upper limits in the 95 % confidence interval for different optical properties are also shown. The trend in the percentage was determined by comparing the slope of the trend with the overall median of the data.

		PM10					PM1				
	λ (nm)	Trend (yr^{-1})		Lower (yr^{-1})	Upper (yr^{-1})	*p*-value	Trend (yr^{-1})		Lower (yr^{-1})	Upper (yr^{-1})	*p*-value
σ_{sca} (Mm^{-1})	550	-0.32	-3 %	-0.52	-0.17	< 0.01	-0.30	-4 %	-0.55	-0.12	< 0.01
σ_{bsca} (Mm^{-1})	550	-0.038	-3 %	-0.070	-0.021	< 0.01	-0.051	-5 %	-0.087	-0.013	< 0.01
σ_{abs} (Mm^{-1})	520	-0.086	-6 %	-0.133	-0.044	< 0.01	-0.141	-12 %	-0.166	-0.098	< 0.01
ω_0	550	2.2e-3	0.3 %	0.7e-3	3.6e-3	< 0.01	5.5e-3	0.6 %	1.5e-3	10e-3	< 0.01
b	550	1.3e-3	0.9 %	0.9e-3	1.7e-3	< 0.01	1.5e-3	1 %	0.7e-3	2.6e-3	< 0.01
α_{sca}	450/700	0.012	0.7 %	-0.001	0.024	0.07	0.014	0.6 %	0.004	0.024	< 0.01
α_{abs}	370/950	-1.5e-4	0 %	-3.0e-3	2.9e-5	0.95	-3.5e-3	-0.3 %	-7.9e-3	13e-3	0.34
n	550	-2.0e-3	-0 %	-3.8e-3	0.6e-3	0.11	-5.7e-3	-0.4 %	-7.5e-3	-2.9e-3	< 0.01
k	550	-6.6e-4	-4 %	-9.1e-4	-3.8e-4	< 0.01	-1.3e-3	-6 %	-2.0e-3	-0.7e-3	< 0.01
$RFE_{H\&S}$ (Wm^{-2})	550	-0.30	-1 %	-0.43	-0.20	< 0.01					
RFE_{S} (Wm^{-2})	550	-0.43	-2 %	-0.64	-0.25	< 0.01					
$RFE_{S,moist}$ (Wm^{-2})	550	-0.3937	-2 %	-0.50	-2423	< 0.01					
N_{tot} (cm^{-3})		-40	-3 %	-52	-28	< 0.01					
V_{tot} (µg cm^{-3})		-0.093	-4 %	-0.120	-0.064	< 0.01					
GMD_{tot} (nm)		-0.092	-0 %	-0.531	0.342	0.63					
VMD_{tot} (nm)		-12	-1 %	-17	-7	< 0.01					

Table 44: Slopes of the seasonal trends and their statistical significance for σ_{sca} and σ_{abs}. The trend in the percentage was determined by comparing the slope of the trend with the seasonal median of the data.

	σ_{sca} (Mm^{-1})					σ_{abs} (Mm^{-1})				
	Trend (yr^{-1})		Lower (yr^{-1})	Upper (yr^{-1})	*p*-value	Trend (yr^{-1})		Lower (yr^{-1})	Upper (yr^{-1})	*p*-value
Spring	-0.44	-5 %	-0.84	-0.04	< 0.05	-0.12	-9 %	-0.20	-0.05	< 0.01
Summer	-0.38	-3 %	-0.79	-0.14	< 0.01	-0.06	-5 %	-0.11	-0.03	< 0.01

Autumn	-0.12	-1 %	-0.49	0.17	0.48	-0.04	-3 %	-0.10	0.03	0.14
Winter	-0.85	-7 %	-1.60	-0.20	< 0.01	-0.17	-8 %	-0.31	-0.03	< 0.05

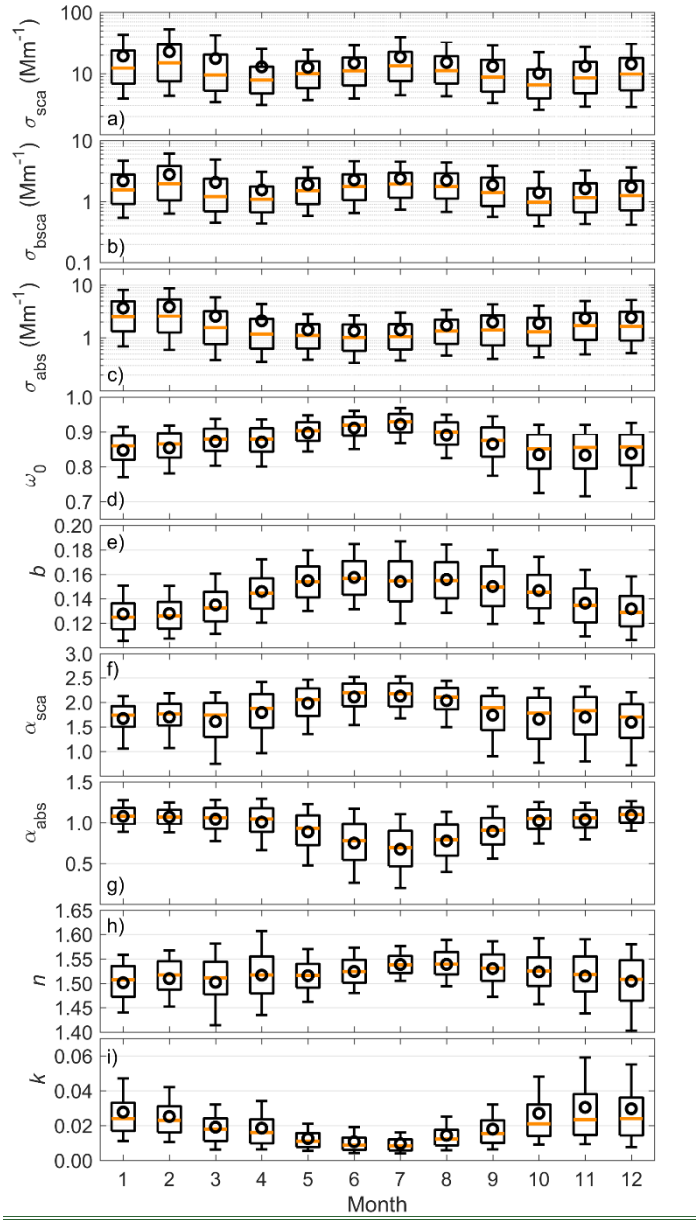

Figure 15: Seasonal variation in the aerosol optical properties for PM10 particles. The boxes represent the 25th and 75th percentiles and the whiskers the 10th and 90th percentiles of the data. The orange line is the median and the mean is presented with a black circle.

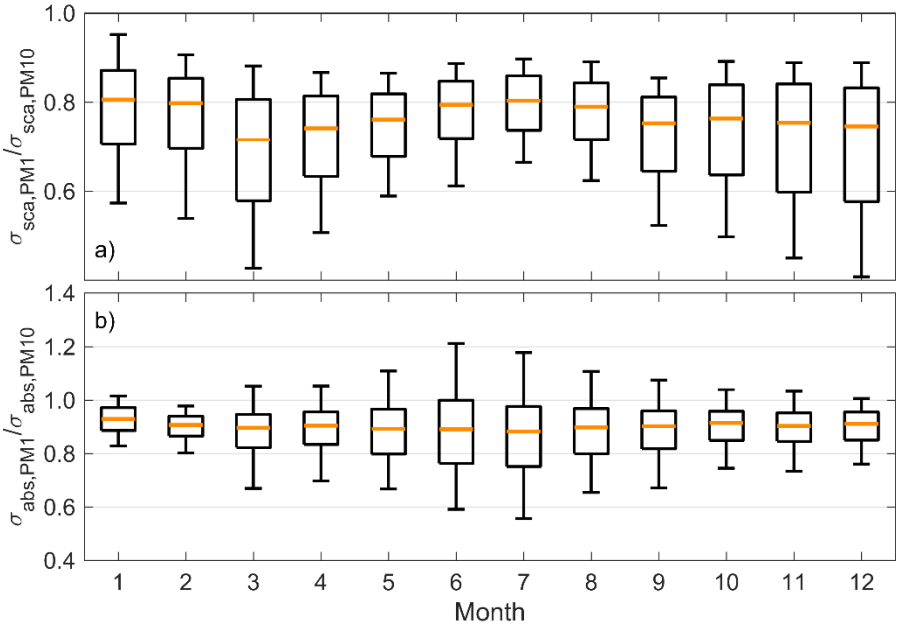

Figure 2~~6~~: Seasonal variation in the PM1/PM10 ratio for a) σ_{sca} and b) σ_{abs}. The explanation for the boxplots are the same as in Fig. 1~~5~~.

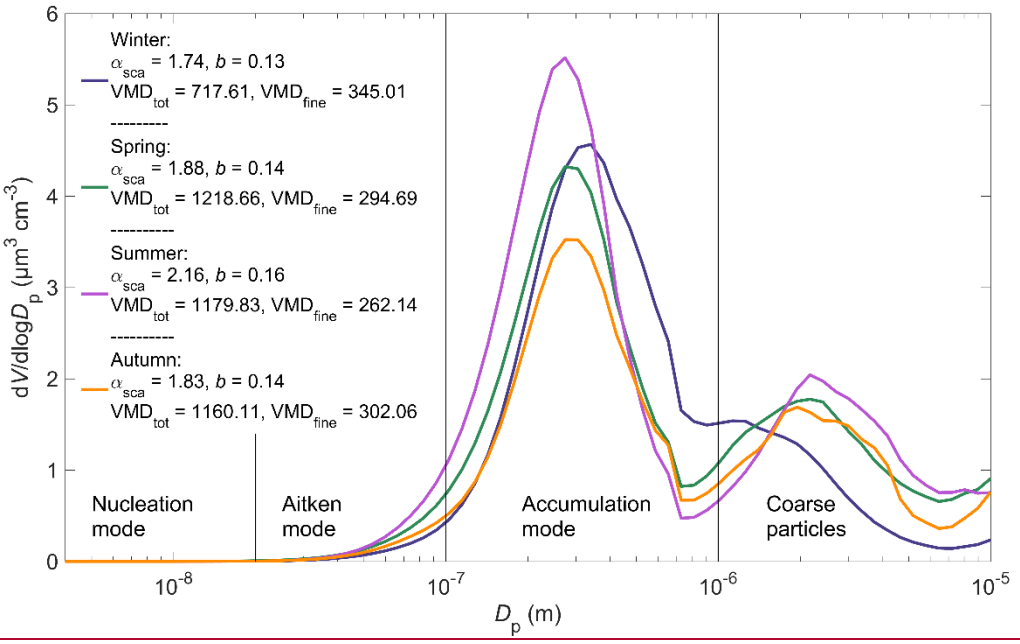

Figure 3: Mean size distribution for winter (December – February), spring (March - May), summer (June – August), and autumn (September – November). Also, the average α_{sca}, b, VMD_{tot}, and VMD_{fine} for the seasons are presented in the figure.

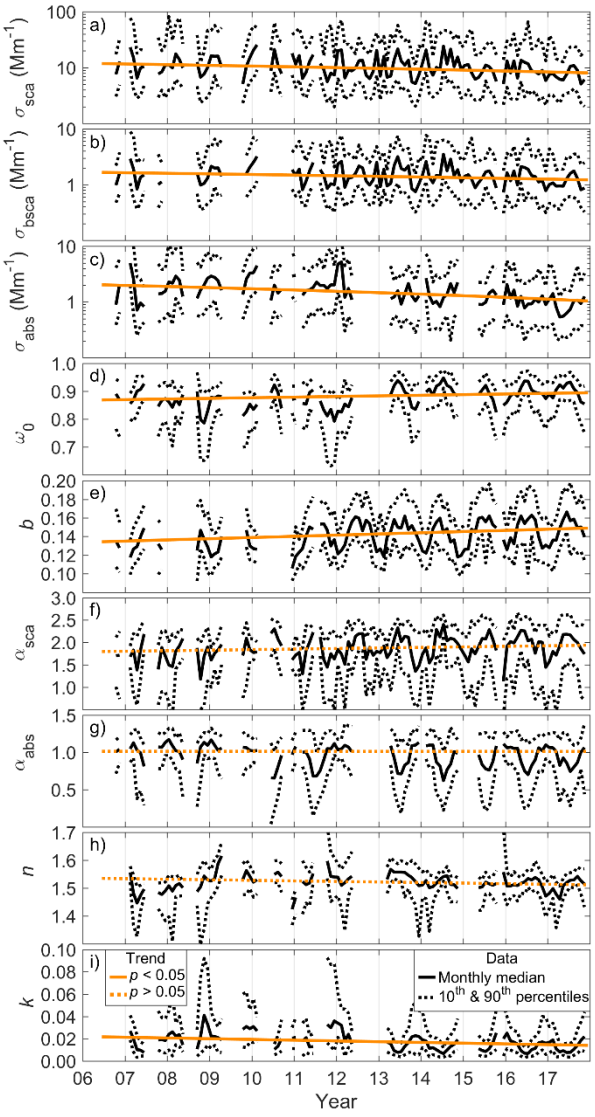

Figure 4: Time series of the PM10 AOPs. The uniform black line presents the monthly median and the dotted black lines present the monthly 10th and 90th percentiles. The trends (see Table 3) of the AOPs are shown with orange lines. If the trend was statistically significant, the line is uniform and if the *p* value of the trend was > 0.05, the line is dashed.

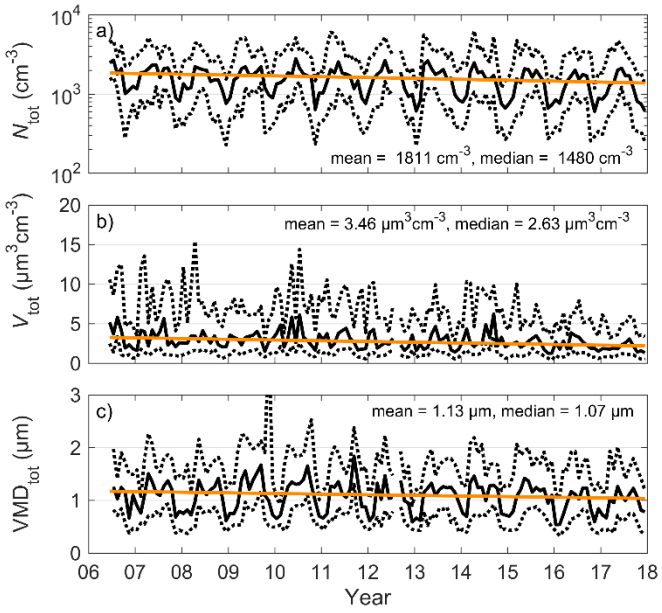

Figure 5: Time series and trends of the total particle (D_p < 10 µm) a) number concentration (N_{tot}), b) volume (V_{tot}) and c) VMD_{tot}. The mean and median values of the variables are also marked in the subfigures and the statistics of their slopes are presented in Table 3. The explanations for the different lines are the same as in Fig. 5~~1~~.

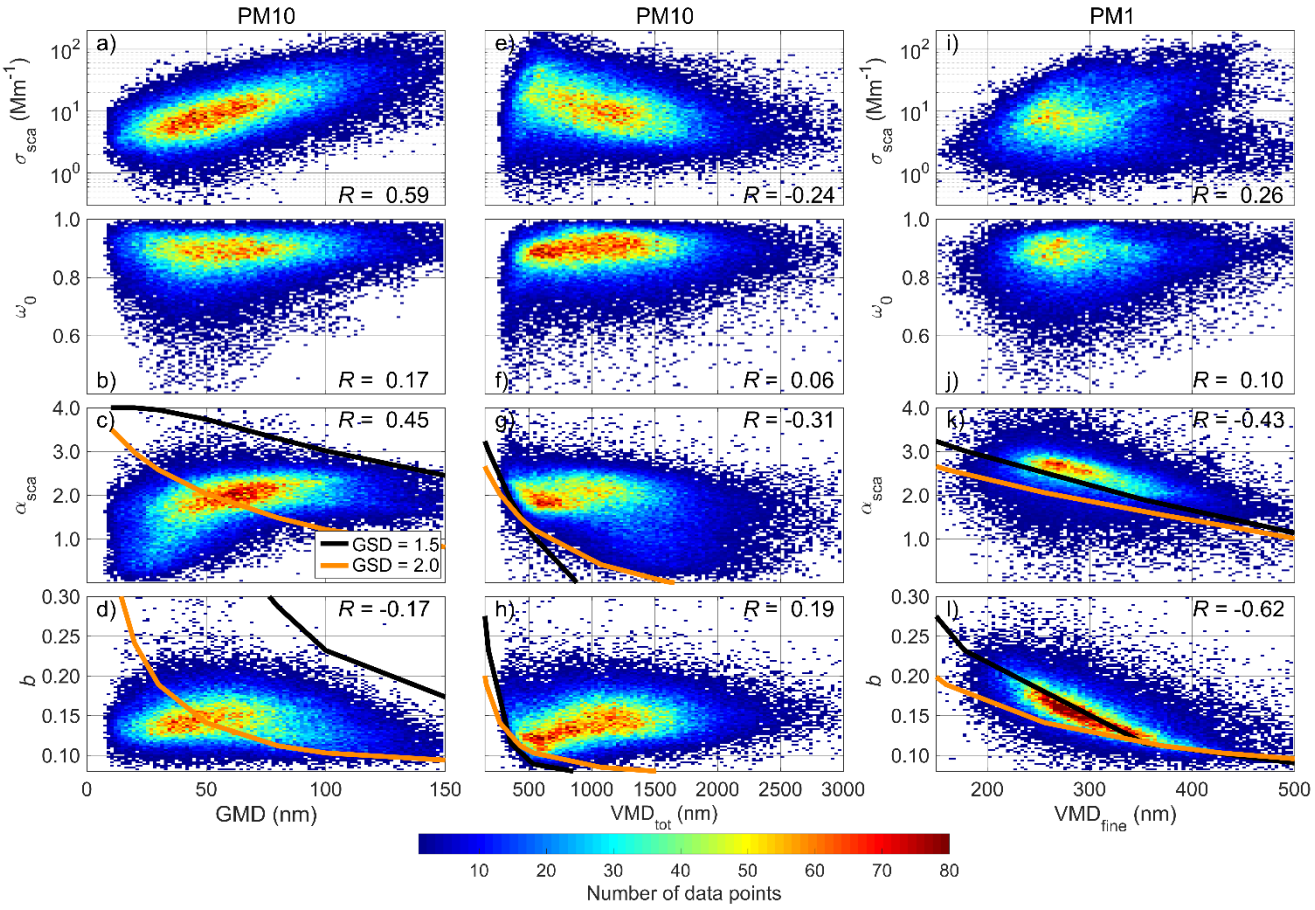

Figure 3: Relationships between the various AOPs, GMD and VMD. Subplots a) – d) describe the correlation between the PM10 AOPs and GMD; subplots e) – h) describe the correlation between the PM10 AOPs and VMDtot; and the subplots i) – l) describe the correlation between the PM1 AOPs and VMD_{fine}. The correlation coefficients of the linear regressions are given in each subfigure. The color-coding represents the number of data points in a grid point. In each subfigure, there are 100 grid points on both axes, making 10 000 grid points in total. The orange and black lines represent the values calculated from the unimodal size distributions, which were generated for different GMDs with geometric standard deviation GSD = 2.0 and 1.5 nm. The scattering was modeled from the generated size distribution at wavelengths 450, 550, and 700 nm with a refractive index $m = 1.517 + 0.19i$.

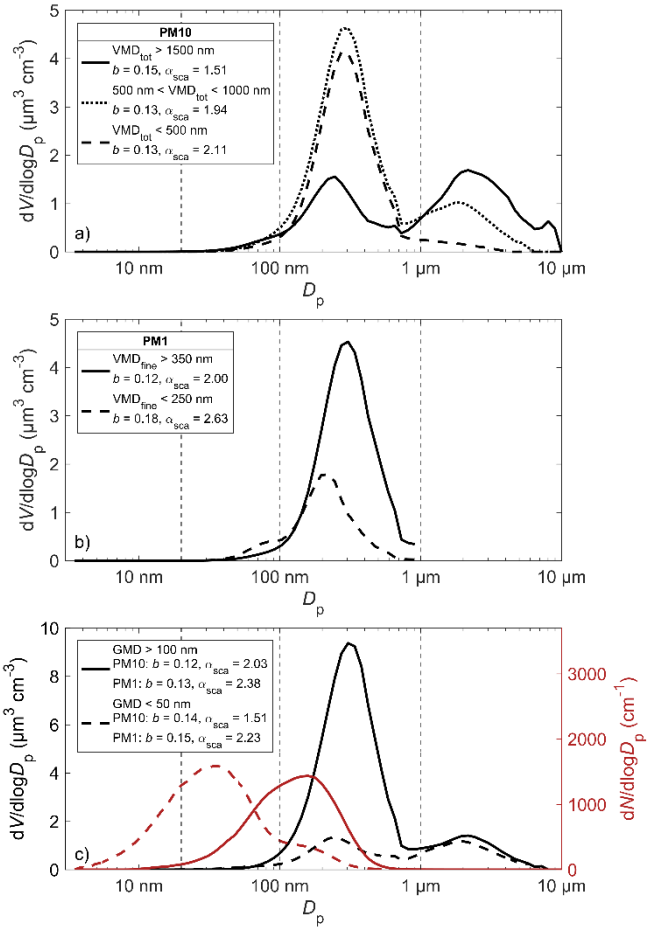

~~**Figure 4: Median volume and number size distributions for the various VMD and GMD limits. The median *b* and α_{sca} for the VMD and GMD limits are given in each legend box. The vertical grid lines represent the typical diameter limits for the nucleation, Aitken, accumulation and coarse particle modes (same as in Figs. S4 and S6). a) Volume size distribution for different PM10 VMD_{tot} limits. b) Volume size distribution for different PM1 VMD_{fine} limits. c) Volume and number size distribution for different PM10 and GMD limits. The c figure also represents volume and number size distribution for different PM1 and GMD limits as well, since the GMD is practically the same for PM10 and PM1 particles.**~~

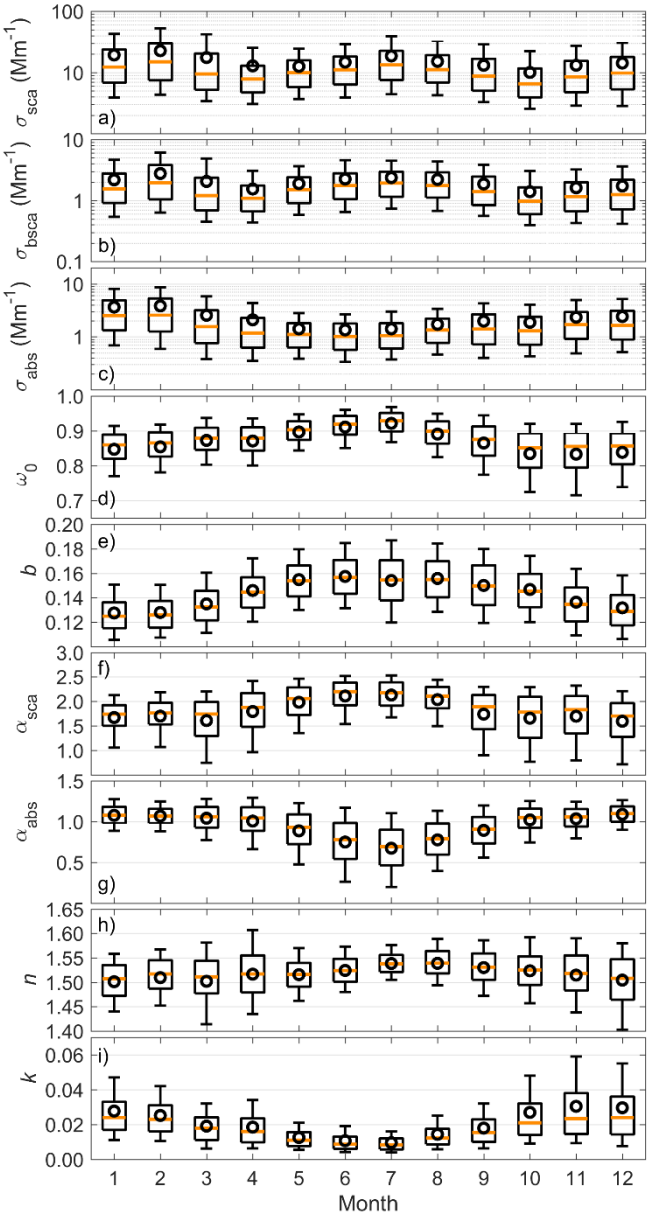

Figure 5: Seasonal variation in the aerosol optical properties for PM10 particles. The boxes represent the 25th and 75th percentiles and the whiskers the 10th and 90th percentiles of the data. The orange line is the median and the mean is presented with a black circle.

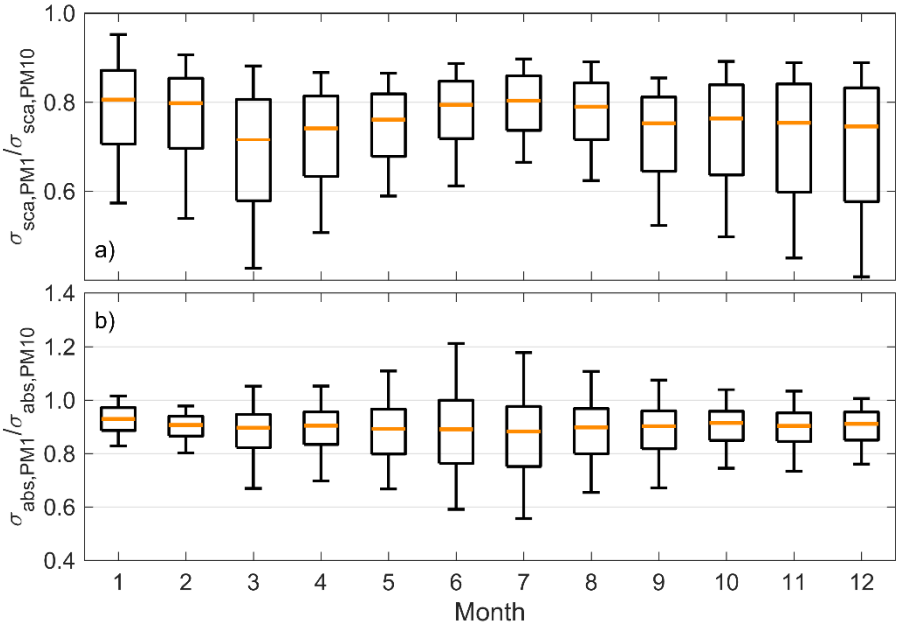

~~**Figure** 6: Seasonal variation in the PM1/PM10 ratio for a) σ_{sca} and b) σ_{abs}. The explanation for the boxplots are the same as in Fig. 5.~~

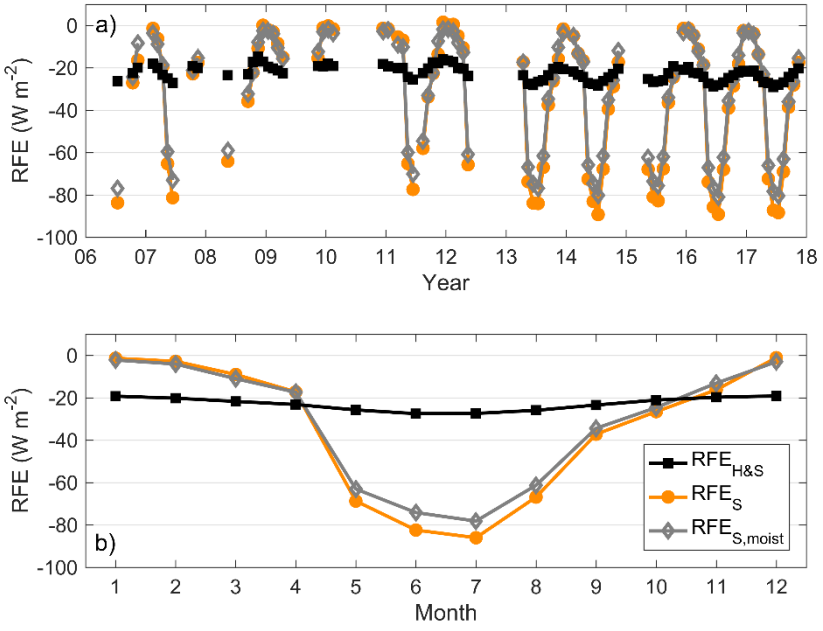

Figure ~~7~~6: Variations in the different radiative forcing efficiencies at SMEAR II in 2006 – 2018. a) Time series of the $RFE_{H\&S}$, RFE_S, and $RFE_{S,moist}$. The monthly medians are presented if the month had at least 14 days of valid data. b) Seasonal variation of the $RFE_{H\&S}$, RFE_S, and $RFE_{S,moist}$ as overall monthly medians. RFE was calculated for PM10 particles.

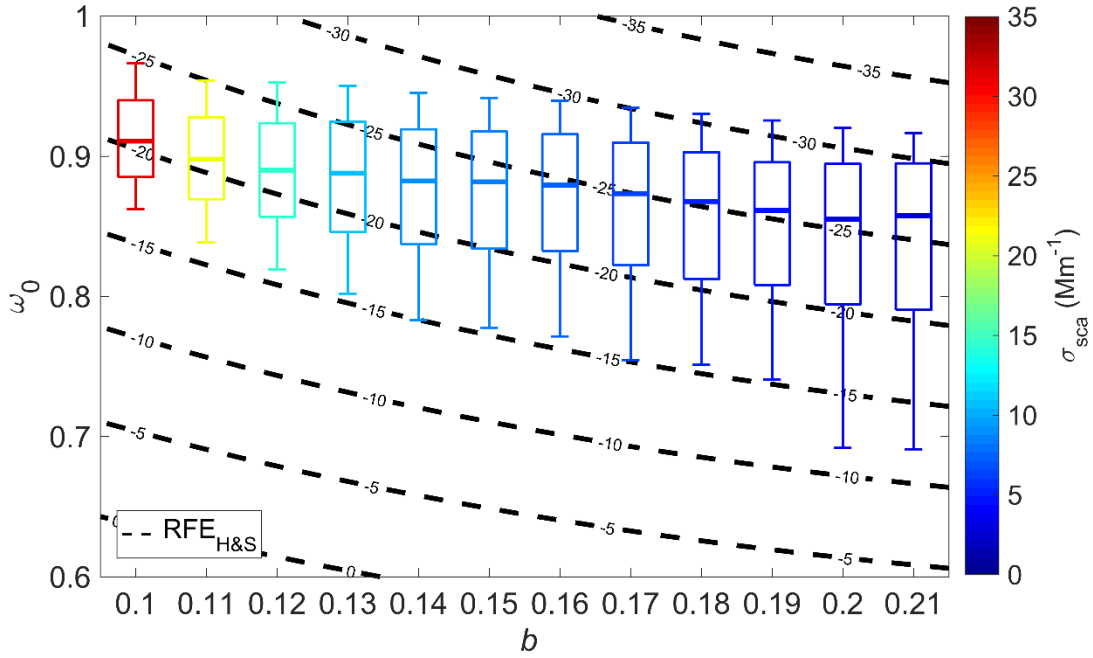

~~Figure 8: Relationships between ω_0, b and RFE$_{H\&S}$. The RFE$_{H\&S}$ is shown as the dashed isolines in the background. The boxes represent the data measured at SMEAR II and they are colored by the median σ_{sca}. The explanation for the boxplots is the same as in Fig. 5.~~